Faculty of Engineering and Architecture
Department of Flow, Heat and Combustion Mechanics

Academic year 2017-2018

Assessment of the performance of mobile fans in a tunnel by flow field measurements and CFD simulations

Mathieu Verpaele

Academic Supervisor: Prof. dr. ir. B. Merci
Academic Co-Supervisor: dr. ir. T. Beji
Industrial Supervisor: ir. X. Deckers

Dissertation nominated to obtain the degree of

The International Master of Science in Fire Safety Engineering (IMFSE)

This thesis is submitted in partial fulfilment of the requirements for the degree of The International Master of Science in Fire Safety Engineering (IMFSE). This thesis has never been submitted for any degree or examination to any other University/programme. The author(s) declare(s) that this thesis is original work except where stated. This declaration constitutes an assertion that full and accurate references and citations have been included for all material, directly included and indirectly contributing to the thesis. The author(s) gives (give) permission to make this master thesis available for consultation and to copy parts of this master thesis for personal use. In the case of any other use, the limitations of the copyright have to be respected, in particular with regard to the obligation to state expressly the source when quoting results from this master thesis. The thesis supervisor must be informed when data or results are used.

read and approved

Version 0.1.0
Compiled on: April 29, 2018

Acknowledgements

I wish to thank my girlfriend and family for giving me the opportunity to do this master and in supporting me through the difficult periods during the thesis. Also a big thank you towards Xavier Deckers to offer me the possibility to perform this thesis and to help looking for solutions when I stumbled upon a problem. During the thesis, Bart Merci was of great help when reviewing the thesis in detail, this helped to fill in the blanks and to enrich the thesis. I want to thank Matteo Pachera as well, he put a lot of time in explaining me certain principles needed for the thesis and giving me access to his 1D network model. The last persons I would like to thank are Jeroen van Beeck and Gertjan Glabeke for taking the time to meet me in the Von Karman institute and helping me figuring out a part of the testing method.

Abstract

Deployment of mobile fans has a big impact in helping to confine the smoke in case of fire in road tunnels. With doing so, increasing the level of security for both drivers and fire fighters. This thesis puts the focus on investigating the performance of mobile fans in a tunnel by means of flow field measurements, a 1D network model and CFD simulations. The mobile fan used for the experiments is a BIG MGV-L105 fan and the experiments were conducted in the Jan De Vostunnel in Belgium. In order to get a correct measurement of the velocity profile in the tunnel a framework was made based on the codes NBN EN 12599 and NBN EN ISO 5802. The framework allows for a detailed comparison with CFD simulations on top of the current comparison of the average velocity for network models. A literature study pointed out that both codes are complementary to each other.

A feasibility study was performed to investigate the performance of the mobile fans in case of fire in a tunnel. Three performance criteria were set: reach a velocity equal or larger than the critical velocity, allow a backlayering length of 30m or 50m. The nine cases considered were a combination of a certain HRR (5MW, 30 MW or 100MW) and the mobile fan set-up(one L105 fan, two L105 fans and one L105 plus one L125 fan). The feasibility study revealed that for an incident tunnel, with one mobile fan and a fire of 5MW, the situation was feasible with an allowance of a limited backlayering length. Wall roughness calculations highlighted the importance of performing pressure measurements over a length L in a zone with an expected constant pressure drop. Especially for tunnels with an irregular cross-section.

Comparison of the measured data with the simulated results lead to several propositions to alter the boundary conditions and thus creating a more accurate simulation. These adaptations involved implementing the louvered vents and changing the length and the number of the eddies, together with changing the root mean square (RMS) velocity fluctuation.

Contents

List of Figures

List of Tables

List Of Symbols

α	slope angle of the tunnel $[degrees]$
$\bar{v}$	mean velocity $[m/s]$
β	local pressure losses $[Pa]$
ΔP_g	pressure losses due to the buoyancy force in the tunnel $[Pa]$
ΔP_{fan}	pressure rise induced by the fan $[Pa]$
ΔP_{fire}	pressure losses by the fire $[Pa]$
ΔP_{wind}	wind pressure $[Pa]$
$\dot{m}$	air mass flow rate $[kg/s]$
η_{inst}	installation efficiency $[\%]$
μ	dynamic viscosity coefficient $[Pa \cdot s]$
ρ_0	air density $[kg/m^3]$
ε	wall roughness $[m]$
A_0	net area of the fan $[m^2]$
A_c	gross area of the fan $[m^2]$
A_t	area of the cross-section of the tunnel $[m^2]$
C_d	discharge coefficient $[-]$
c_p	thermal capacity of air $[kJ/kgK]$
D_f	inner free diameter of the fan $[m]$
D_h	hydraulic diameter, $D_h = 4A/P$ for rectangular cross-sections $[m]$
f	friction coefficient $[-]$
g	gravitational acceleration $[m^2/s]$
H	height of the tunnel $[m]$
h	lumped transfer coefficient $[kW/m^K]$
I^*	dimensionless backlayering length $[-]$

$K^{'}$	constant,$K^{'} = 1.13K = 7$, $K = 6.2$ for round openings with an outlet velocity between 10 and 25m/s [−]
k_p	coverage factor for a normal or rectangular distribution [−]
L_t	length of the tunnel $[m]$
L_{bl}	backlayering length $[m]$
P	perimeter of the tunnel $[m]$
p_l	Inverse of the exponent of the characteristic law of the evolution of velocities at the wall (taking into account the measurement results of the surface roughness of the walls and the value of the Reynolds numbers [2])
Q^*	dimensionless HRR [−]
Q_0	suplly volume flow rate $[m^3/s]$
R_{fa}	ratio of the free area over the gross area of the outlet [−]
Re_D	Reynolds number [−]
T_{amb}	ambiant temperature $[K]$
T_{fire}	fire temperature $[K]$
U	irregularity of the velocity profile [%]
u_{pr}	standard uncertainty of the measuring equipment for velocity $[m/s]$
V_c	critical velocity in a tunnel $[m/s]$
V_c*	dimensionless critical velocity in a tunnel [−]
v_f	fan outlet velocity $[m/s]$
v_t	velocity in the tunnel $[m/s]$
V_x	centreline velocity $[m/s]$
v_{wind}	wind velocity $[m/s]$
x	abcis-axis
X_t	throw length of a fan $[m]$
y	ordinate-axis

Introduction

Current measuring protocols for the measurement of the velocity of air in underground structures are basic. They are mainly intended to check if the critical velocity as required by the design is met. The accuracy of the measuring methods is often not sufficient to describe the velocity distribution over the cross section in a detailed manner and can thus not be used to improve the boundary conditions in the CFD-design. This thesis will try to find a uniform framework for flow field measurements in all types of underground structures (road tunnels, rail tunnels, underground parking, etc.) and will try to couple the CFD-design to that framework. The aim of this coupling is to reduce the measuring time needed for a sufficiently accurate result, with also a faster modelling time. A balance for the cost-benefit is investigated.

In Belgium there are currently three codes explaining the methods for measuring the velocity in a channel. The codes reviewed in this thesis will be: NBN EN 12599 [1](Ventilation for buildings - Test procedures and measurement methods to hand over air conditioning and ventilation systems), NBN EN ISO 5802 [2] (Industrial fans - Performance testing in situ (ISO 5802:2001)) and NBN S 21-208-2 [3](Fire protection in buildings - Design of smoke and heat exhaust ventilation systems (SHEV) for enclosed car park). The third code will not be used to determine the final framework, but will be used to point out the inaccuracy of some of the current measuring methods.

With this framework a number of flow field experiments were conducted in the Jan De Vos-tunnel in Belgium to improve the boundary conditions of the CFD-simulations from the tunnel.

The Fire Brigade Zone Rand owns a mobile fan for the smoke and heat control of large hangars and industry halls. The mobile fan can also be used for the smoke and heat control of road tunnels. However, the use of mobile units for an intervention as such has not been focused on in the current literature.

Given that the condition of road tunnels in Belgium that are already long in use can be poor, additional risks can emerge in case of fire. Hence, it is certainly useful to perform flow field measurements to investigate in which situation the mobile fan can improve the risk-level and provide sufficient safety for people present in the incident tunnel. To express the practical use of such mobile fans, a feasibility study was performed indicating in which situations the mobile fans prove to be an added value.

The set-up and use is different than that of the standard booster hanging in regular road tunnels. This thesis will focus on the mapping of the flow field with different types of measuring grids to find the coarsest grid possible with still a high enough accuracy to draw reliable conclusions. Afterwards, the boundary conditions of CFD simulations of the mobile unit and the tunnel will be improved with the collected data. This way, future ventilation simulations of an incident tunnel can be more accurate.

The first part of the experiments were done in cold conditions. The second part will be done in hot conditions but will not be further discussed in this thesis, the experiments take place in August . The aim of the hot experiments will be to calculate the convective heat of two cars burning in an underground parking lot equipped with sprinklers. The same framework as for the cold conditions will be used.

Chapter 1

The codes

1.1 NBN EN 12599: Ventilation for buildings - Test procedures and measurement methods to hand over air conditioning and ventilation systems [1]

1.1.1 General

This code is used for measuring inside ducts, at the end of a fan and in rooms (this is not included in this dissertation considering these specific measurements are focused on velocities on heights that can be felt by humans, max. 2m). Although a duct and a tunnel are two different things in size and use, the velocity profile is assumed to be similar. The measuring procedure, described as the simple method, has a limited additional value. On the other hand, the way the code handles measuring equipment and the uncertainties coming with it, are of importance for the comparison with the FDS simulations. The uncertainties will be separately discussed in Chapter 2.

Determining the velocities at a specified location in the tunnel is accomplished with a measuring grid. To make sure that the measurements are valid, it is important to have a measuring grid at place where the velocity profile is stable and where no large turbulences are present.

1.1.2 Measuring method

EN 12599 uses the simple method, This method covers all measuring methods in which special assumptions cannot be made about the velocity profile. The velocity is measured point by point along any desired number of measurement lines. The grid size depends on the geometry of the cross-section and the velocity profile. For measurements with high velocity it is preferable to increase the number of measuring points. The philosophy of the set-up of the grids is the creation of zones of equal area with one probe per zone, and calculating the arithmetic mean afterwards.

The simple method can be used for rectangular and circular cross-sections. In both sections,

a grid will be set up. This grid will have a probe in the middle of every zone of equal are. For circular cross-sections, the probes will be installed on diameters perpendicular to each other for neighbouring annuli. The distances of the grid points depend on how many measurements lines and columns are used for the measurement. Below, in figures 1.1 and 1.2, the different options for a grid are presented. Table 1.1 shows the relative distances between the measuring points for a rectangular grid. Table 1.2 and Table 1.3 show the relative distances for the circular cross-section.

After measurement, the arithmetic mean is taken of all the values and one value is the output value. This could be useful network model calculations where a single velocity is required.

The measurement should be done for at least 100 second. In environments with large fluctuations, 180 seconds is the timespan per measurement.

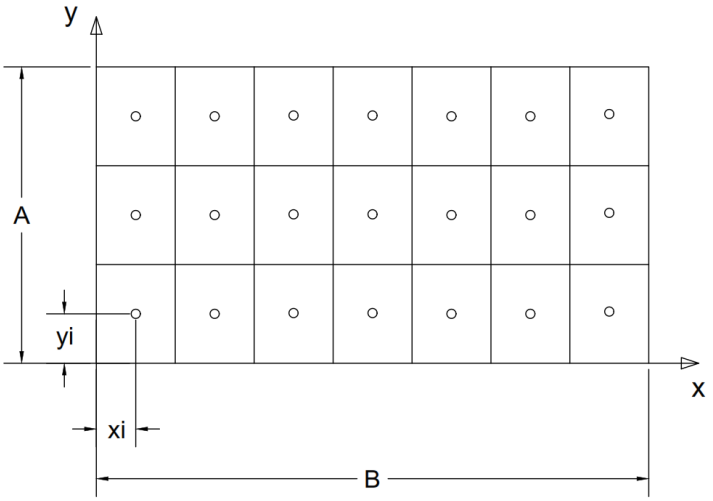

Figure 1.1: Representation of the division of a rectangular cross-section in parts of equal area, redrawn from [1]

Table 1.1: Relative wall distances of measuring points for a rectangular grid [1], x_i and y_i as illustrated in Figure 1.1

Number of measuring points for each measuring straight line	Measuring point i, $\frac{x_i}{B}$ or $\frac{y_i}{A}$									
n	1	2	3	4	5	6	7	8	9	10
3	0.167	0.500	0.633							
4	0.125	0.375	0.625	0.875						
5	0.100	0.300	0.500	0.700	0.900					
6	0.083	0.250	0.417	0.583	0.750	0.917				
7	0.071	0.214	0.357	0.500	0.643	0.786	0.929			
8	0.062	0.187	0.312	0.438	0.563	0.688	0.813	0.938		
9	0.056	0.167	0.278	0.389	0.500	0.611	0.722	0.833	0.944	
10	0.050	0.150	0.250	0.350	0.450	0.550	0.650	0.750	0.850	0.950

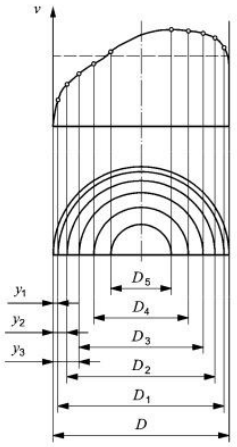

Key

D_i centroidal axis diameter

y_i distance from wall

v velocity

Figure 1.2: Representation of the division of a circular cross-section in parts of equal area [1]

Table 1.2: Relative wall distance of the centroidal axes $\frac{y_i}{D}$, y_i and D as illustrated in Figure 1.2

i n	1	2	3	4	5	6	7	8	9	10
1	0.1464									
2	0.0670	0.2500								
3	0.0436	0.1464	0.29595							
4	0.0323	0.1047	0.1938	0.3232						
5	0.0257	0.0817	0.1464	0.2261	0.3419					
6	0.0213	0.0670	0.1181	0.1773	0.2500	0.3557				
7	0.0182	0.0568	0.0991	0.1464	0.2012	0.2685	0.3664			
8	0.0159	0.0493	0.0854	0.1250	0.693	0.2205	0.2835	0.3750		
9	0.0141	0.0436	0.0751	0.1091	0.1464	0.1882	0.2365	0.2959	0.3821	
10	0.0127	0.03950	0.0670	0.0969	0.1292	0.1646	0.2042	0.250	0.3064	0.3882
Note:	$\frac{y_i}{D} = \frac{1}{2}(1 - \sqrt{(}1 - \frac{2i-1}{n}))$									

Table 1.3: Relative centroidal axis diameter $\frac{D_i}{D}$, y_i and D as illustrated in Figure 1.2

i n	1	2	3	4	5	6	7	8	9	10
1	0.7071									
2	0.8660	0.5000								
3	0.9129	0.7071	0.4082							
4	0.9354	0.7906	0.6214	0.3536						
5	0.9487	0.8367	0.7071	0.5477	0.3162					
6	0.9574	0.8660	0.7638	0.6455	0.500	0.2887				
7	0.9636	0.8864	0.8018	0.7071	0.5976	0.4629	0.2673			
8	0.9682	0.9014	0.8292	0.7500	0.6614	0.5590	0.4330	0.2500		
9	0.9718	0.9129	0.8498	0.7817	0.7071	0.6236	0.5270	0.4082	0.2357	
10	0.9747	0.9220	0.8660	0.8062	0.7416	0.6708	0.5916	0.5000	0.3873	0.2236
Note:	$\frac{D_i}{D} = \sqrt{(}1 - \frac{2i-1}{n})$									

1.2 NBN EN ISO 5802: Industrial fans Performance testing in situ [2]

1.2.1 General

This code is written in the need of a stand-alone document for the in situ performance testing of industrial fans. As was mentioned in the part about EN 12599, it is assumed that the velocity profile of a duct is similar to that of a tunnel. Since this document is focused on the in situ performance testing, it takes in account the different duct shapes possible. Industrial use does not only mean the use of fans in industries but has a broader field of interpretation. Industrial fans can also be used in tunnels, underground car parks,etc... In general, facilities that are often underground where the ducts can be integrated upon construction of the facility. In this way, ducts can have different shapes than the conventional rectangular and circular shape of a standard duct. An important detail that is mentioned very clearly in the introduction of the code is that instead of using the simple method of EN 12599 for measuring velocities, the code proposes the log-Tchebycheff or log-linear distribution of the measuring points. This distribution is intuitively more preferable when looking at a velocity profile in a duct/tunnel.

1.2.2 Measuring methods

As mentioned in the general description, the log-Tchebycheff or the log-linear method is chosen for the allocation of the probes. In papers presented on the conferences in Graz [6] and the BHR symposia[7][8], the log-Tchebycheff approach is most often used and for this reason only the log-Tchebycheff distribution will be analysed in this dissertation. In the sections below, the different approaches for determining the measuring grid are explained. Once the grid is resolved and measurements are done, the next step is to calculate the arithmetic mean. The mean velocity times the area of the section gives the volumetric flow rate.

1.2.2.1 Standard cross-sections

For the circular grid, a minimum of 24 measuring points is required. The relative distances for three points per radius are shown in Table 1.4 and in Table 1.5 for four points (32 measuring points). The rectangular grid requires a minimum of 25 measuring points. The amount of cross-lines and the amount of points on each cross-line should not be less than five. Table 6 shows the relative distances for a rectangular cross-section.

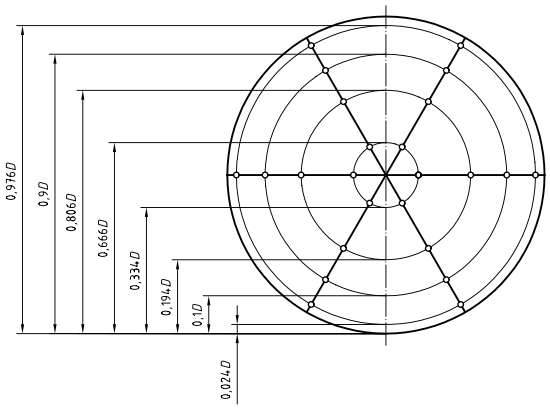

Figure 1.3: Example of a grid in a circular cross-section according to the Log-Tchebycheff distribution [2]

Table 1.4: Three points per radius grid for a circular cross-section [2]

Point	Log-Tchebycheff y/D
1	0.032
2	0.137
3	0.312
4	0.688
5	0.863
6	0.968

Table 1.5: Four points per radius grid for a circular cross-section [2]

Point	Log-Tchebycheff y/D
1	0.021
2	0.100
3	0.194
4	0.334
5	0.666
6	0.816
7	0.883
8	0.979

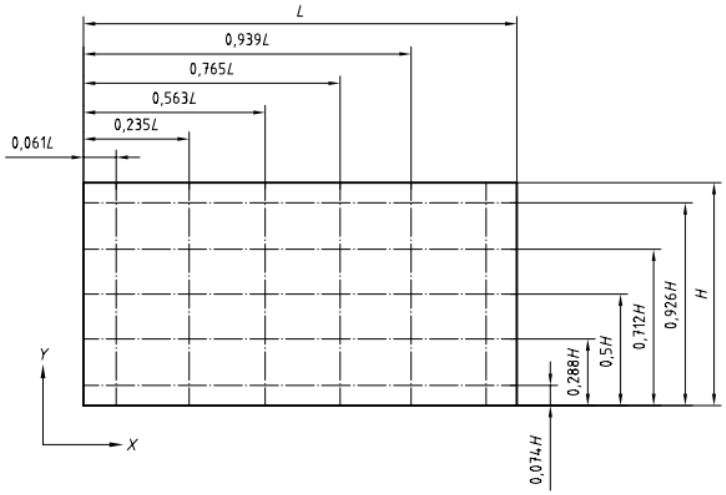

Figure 1.4: Example of a grid in a circular cross-section according to the Log-Tchebycheff distribution [2]

Table 1.6: Point and line distribution of a rectangular cross-section [2]

Number of cross-lines or number of measuring points per cross-line	Point	Values of $\frac{x_i}{L}$ or $\frac{y_i}{H}$
5	1	0.074
	2	0.288
	3	0.500
	4	0.712
	5	0.926
6	1	0.061
	2	0.235
	3	0.437
	4	0.563
	5	0.765
	6	0.939
7	1	0.053
	2	0.203
	3	0.366
	4	0.500
	5	0.634
	6	0.797
	7	0.947

1.2.2.2 Non-standard sections

In case of tunnels, the cross-sections are often not the standard rectangular or circular cross-sections. When the shape of the cross-section changes, the velocity profile will change and it is thus important that the velocities measured near the wall are measured at the right position to be able to approximate the true velocity profile in the same manner as with the standard cross-sections. The traverse lines in between the marginal traverse lines are assumed to follow the same distribution as the standard cross-section. Since the relative distances for the cross-lines given in Table 1.6 are only suitable for the standard rectangular cross-sections, there is need for a different procedure to determine the relative wall distance of the marginal traverse lines.

1.2.2.3 Simple solution for the relative wall distance of the marginal traverse lines

For cross-sections different from the standard rectangular or circular cross-sections the log-Tchebycheff traverse pattern is used to determine the positioning of the probes. The code describes a step-to-step guideline to follow when dealing with a non-standard cross-section:

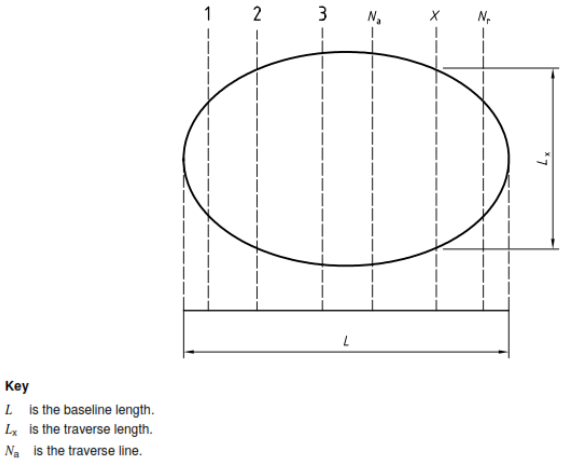

Figure 1.5: Non-standard cross-section showing sample distribution of traverse lines [2]

Table 1.7: Value of p_l as a function of roughness og the walls and of the Reynolds number [2]

Rough wall with low Reynolds number	p_l=5
Rough wall with high Reynolds number or Smooth wall with low Reynolds number	p_l=7
Smooth wall with high Reynolds number	p_l=10

1. A baseline shall be chosen parallel to the major axis of the duct cross-section. In most cases this is the horizontal x-axis.

2. Velocity measurements shall be taken at prescribed points along at least six parallel traverse lines at right angles to the baseline and at right angles to the axis of flow. Lines 1 to N_r in Figure 1.5.
3. Traverse lines numbers 2 to (N_r - 1) shall be distributed along the baseline according to the log-Tchebycheff rule, see Table 1.6.
4. Traverse lines 1 and N_r shall be placed in accordance with the appropriate table adjacent to Figure A.1 to Figure A.13 in Appendix A . The value of p_l in these tables shall be selected from Table 1.7 and if no specific determination of wall roughness can be made, then the value p_l=7 should be used.
5. At least six measuring points shall be located along each traverse line in accordance with the log-Tchebycheff rule, see Table 1.6 Where any traverse line is very short, the number of measuring points may be reduced to five but the total number of measuring points for the whole area shall not be less than 35.

1.2.2.4 General calculation of the relative wall distance of marginal traverse lines using graphs

For cases where the figures A.1 to A.13 in Appendix A do not apply, which will be the case for most of the tunnel cross-sections, the code describes how to calculate it based on an equation

$$y = kx^{\frac{-1}{p_l}} \tag{1.1}$$

Where p_l is equal to 7 and k varies from 0 to 1.

This calculation works with 7 traverse lines.

Step 1 is to plot the family of curves of equation (1.1) in a graph with X/a as measuring unit for the abcis and Y/a or l_i/a for the ordinate, see also Figure 1.6. "The width of the base up to the vertical line of abscissa 1 represents the dimensionless width a/a of the cross-section being considered."[2]

Step 2 is to plot the different vertical dimensionless heights l_1/a to l_5/a at the following abscissae and plot a curve connecting the values:

ordinate values	l_1/a	l_2/a	l_3/a	l_4/a	l_5/a
abscissa values	0.054	0.242	0.509	0.774	0.954

Step 3, sum up the dimensionless heights and determine I/a as follows:

$$\frac{I}{a} = 0.083\frac{l_1}{a} + 0.196\frac{l_2}{a} + 0.255\frac{l_3}{a} + 0.266\frac{l_4}{a} + 0.155\frac{l_5}{a} \tag{1.2}$$

Step 4, plot I/a at abscissa = 1and draw a curve parallel with the family of curves to intersect the curve from step 2. The abscissa of that intersection point equals b/a. In this way b can be found and thus the distance from the wall for traverse lines 1 and N_r.

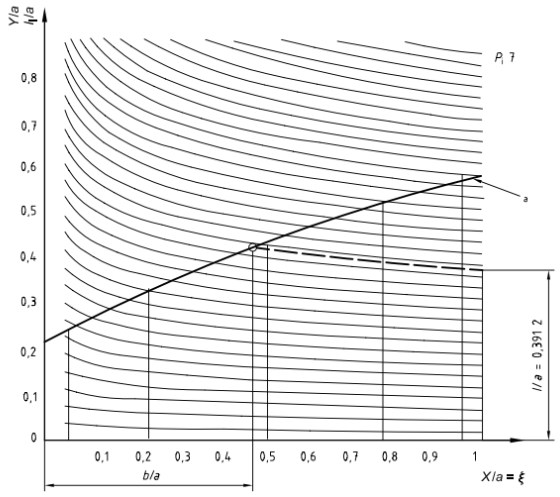

Figure 1.6: Example graph with the family curves and the dimensionless heights and widths [2]

1.2.2.5 Specific calculations of the relative wall distance of marginal traverse lines for cross-sections with only decrease of height in the corners

A couple of tunnels in Belgium have a cross-section where the top corners of the cross-section are curved or are chamfered. The length where there is a various height is often limited to 10% of the width of the section. The remainder 90% of the heights are the full height of the section. When using the previous sub chapter, the results can have some read out error of the graph since it is assumed that the corners are curved. It does not take in account that the corners can be inclined straight lines. The code describes a calculation procedure for the determination of relative wall distance of marginal traverse lines, for cases where only corners show a various height or as the codes describes it: wall profiles compatible with a general power law. The law that is followed:

$$l_x = l_0 + (l_a - l_0)\frac{x}{a}^{\frac{1}{p_l}} \tag{1.3}$$

Where:

- l_x: the length at the running abscissa x
- l_0: the length at abscissa $x = 0$
- l_a: the length at the abscissa $x = a$ (a = length)

In the code a is defined as: $a = L/m_l$ with m_l = number of cross-lines. It should be kept in mind that this is in function of ducts. The proportions of the length of the curved corner are different for a duct than for a tunnel. Though it should always be checked if a does not exceed L/m_l. Then it is best to work with the graph method.

For curved corners (example see Figure 7) the relative position z($\frac{b}{a}$) of the marginal traverse

line may be calculated from the transcendental equation:

$$z^{\frac{1}{p_l}}[l_0 + (l_a - l_0)z^{\frac{1}{p_l''}}] = l_0\frac{p_l}{p_l + 1} + (l_a - l_0)\frac{p_l''}{p_l'' + 1} \tag{1.4}$$

With:

$\frac{1}{p_l''} = \frac{1}{p_l} + \frac{1}{p_l'}$

$p_l' = \frac{AC}{AB}$; Point B is the intersection of the ordinate axis and the tangent in $x = a$

p_l see Table 1.7

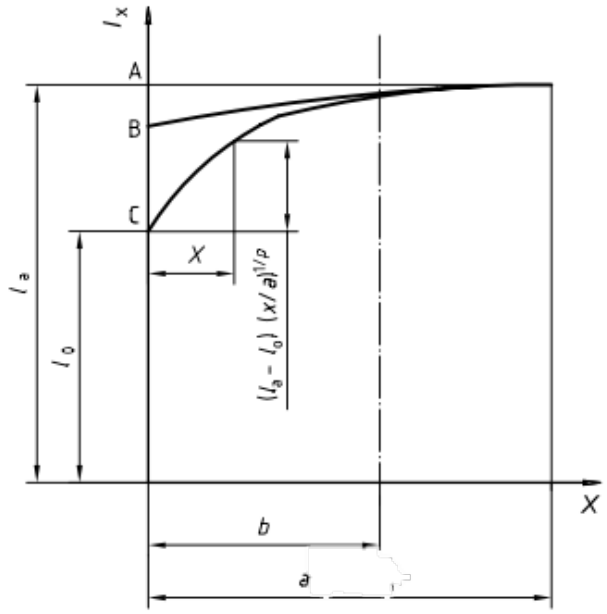

Figure 1.7: Schematic of the location of the marginal traverse line for curved corners[2]

For chamfered corners, the expression for the relative wall distance z is defined as:

$$z^{\frac{1}{p_l}}[l_0 + (l_a - l_0)z] = l_0\frac{p_l}{p_l + 1} + (l_a - l_0)\frac{p_l}{2p_l + 1} \tag{1.5}$$

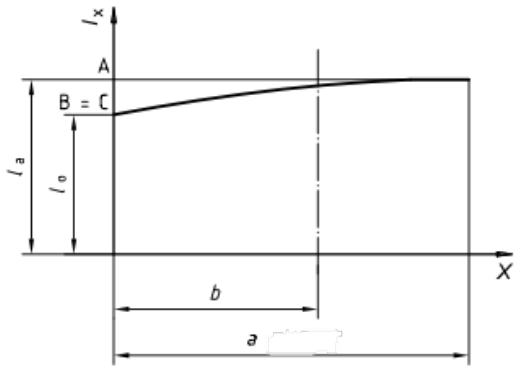

Figure 1.8: Schematic of the location of the marginal traverse line for chamfered corners, [2]

1.3 NBN EN ISO 5802: Design of smoke and heat exhaust ventilation systems (SHEV) for enclosed car park [3]

1.3.1 General

This code has as purpose to determine the design of smoke and heat exhaust systems for enclosed car parks with one or more levels such that the spread of smoke and heat is limited when a fire occurs, and to ensure a safe path for the fire brigade to extinguish the fire. Different types of design are described to ensure the basic requirements. This code is not meant for the design of daily ventilation of car parks.

1.3.2 Measuring methods

The measurements are to be executed in cold conditions with a wind velocity lower than 4 m/s, using the loop method. The loop method is said to be based on the EN 12599, although this seems doubtful since the EN 12599 uses a measuring grid and the loop method exists of scanning with one probe on three levels. The three levels are located on 1/4, 1/2 and 3/4 of the height on that location, see also Figure 1.9. The scanning of one level has a duration of 30 seconds and the minimum distance of the walls is set to be 0.5 m. When using boosters attached at the ceiling without mechanical air exhaust, the measurements should be done twice, once at zero wind speed and once at a wind speed higher or equal than 5 m/s at 10m above ground level.

1.4 Summary

For the remainder of the thesis the norm NBN EN ISO 5802 will be used as a guideline to set up the measuring grid. The Log-Tchebycheff method is the most realistic to map the velocity profile in a correct manner. This method takes into account the steep raise in velocity from the boundaries (where the velocity is 0 m/s) to a zone close to the boundaries. The norm

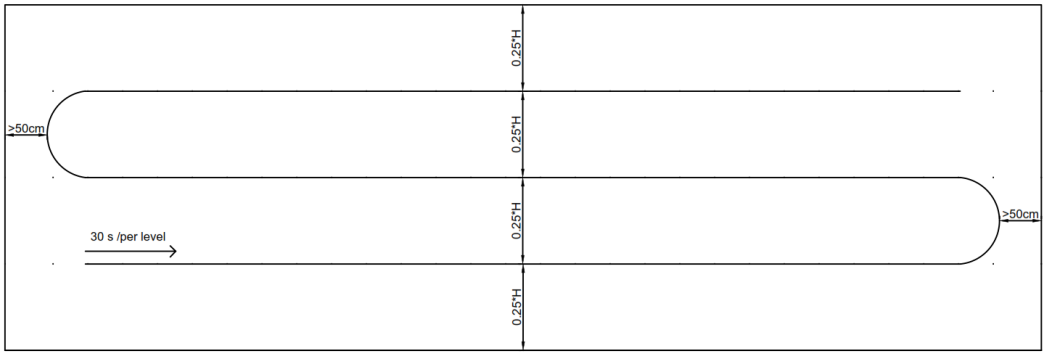

Figure 1.9: Schematic of the loop method

NBN S21-208-2 is advised not to apply when the possibility exists of measuring with a grid. The uncertainty of the loop method is hard to define and will be higher than the previous mentioned methods since it is a human being moving the probe with a supposedly constant velocity on three different levels.

Chapter 2

Uncertainties

Vocabulary [9]

- Measurand: particular quantity subject to measure
- True value: value consistent with the definition of a given particular quantity; a value that would be obtained by a perfect measurement
- Error: result of a measurement minus a true value of the measurand
- Random error: result of a measurement minus the mean that would result from an infinite number of measurements of the same measurand carried out under repeatability conditions; error minus the systematic error
- Systematic error: mean that would result from an infinite number of measurements of the same measurand carried out under repeatability conditions minus a true value of the measurand; error minus random error.

2.1 How to deal with uncertainties of measurements

When performing a measurement, the measurement result is not the true value of the measurand. Random and systematic errors occur during the test. Whereas the exact value of those errors is unknown and unknowable, the uncertainties that come with random and systematic errors make that the errors can be evaluated. Although the errors can be evaluated, when the uncertainty is small it doesnt mean that the error in the measurement result is small. In the evaluation of the errors, a systematic error can be overlooked and as described in JCGM 100:2008 (GUM 1995 with minor corrections, Evaluation of measurement data - Guide to the expression of uncertainty in measurement) [9]: "the uncertainty of a result of a measurement is simply an estimate of the likelihood of nearness to the best value (of the measurand) that is consistent with presently available knowledge".

"Uncertainty of measurement is thus an expression of the fact that, for a given measurand and a given result of measurement of it, there is not one value but an infinite number of

values dispersed around the result that are consistent with all of the observations and data and ones knowledge of the physical world, and that with varying degrees of credibility can be attributed to the measurand."[9]

To mitigate errors the test set-up should comply with certain repeatability conditions. Those repeatability conditions include the same measurement procedure, the same observer, the same measuring instrument (used under the same conditions), the same location and repetition over a short period of time.[9]

For the remainder of this dissertation, only uncertainties of measurements will be used to evaluate the results. The uncertainties mentioned will be translated to relative uncertainties, in order to be able to calculate the total uncertainty. Standard uncertainties can be evaluated in two ways, a type A evaluation or a type B evaluation. A type A evaluation is the method where uncertainty is evaluated by the statistical analysis of series of observations, whereas a type B evaluation is the method where uncertainty is evaluated by other means than the statistical analysis of series of observations. Type B will be used in this dissertation to determine the uncertainties of the measuring equipment and the uniformity of the velocity profile. Type A is more often used in the calibration process of measuring equipment.

2.2 Uncertainties of measuring equipment

Measuring equipment is usually calibrated in the factory and the measuring uncertainty given after the calibration is often noted as a tolerance interval with a given level of confidence. The distribution in that interval is assumed to be a normal distribution. This tolerance interval can be converted to a standard uncertainty using following formula:

$$u_{pr}(x_i) = \frac{\Delta x}{k_p} \tag{2.1}$$

With:

$u_{pr}(x_i)$:	standard uncertainty of the measuring equipment for velocity measured at $probe_i$
Interval:	$[x \pm \Delta x]$
k_p:	coverage factor for a normal or rectangular distribution, see also Table 2.1 and Table 2.2.

Table 2.1: Value of the coverage factor for a certain interval having a level of confidence p and a normal distribution

Level of confidence p [%]	k_p
68.27	1
90	1.645
95	1.960
95.45	2
99	2.576
99.73	3

Table 2.2: Value of the coverage factor for a certain interval having a level of confidence p and a rectangular distribution

Level of confidence p [%]	k_p
57.74	1
95	1.65
99	1.71
100	1.73

2.3 Uncertainties of the velocity profile

In a channel, tube or tunnel the walls are not always perfect clear of obstacles or the friction factor can change for the different walls. To mitigate the influence of large upstream objects it is best to measure as far away as possible from those upstream obstacles/disturbances. The EN 12599 gives a rule of thumb to estimate those distances and the corresponding uncertainties in function of the amount of measuring points, see Table 2.3 below. This Table was created originally to determine the amount of required measuring points for a specific level of uncertainty. This can also be looked at in an inverted way, by looking at the relative distance from a disturbance in function of the relative uncertainty and the amount of measuring points. EN ISO 5802 requires the minimum distance from the fan outlet to be five times the hydraulic diameter of the duct, this is in case of industrial fans with measurements in ducts. Both codes represent the same idea, the farther away from the fan outlet or large obstacles, the better the results. This will be applied for the measurements as an indication of the location of the grid.

Table 2.3: Required numbers of measuring points as a function of the relative distance from a disturbance and the relative uncertainty [1]

Required number of measuring points			
Relative distance	Total uncertainty [%]/uncertainty of the measuring device [%]		
a/D_h	"10/5"	"15/5"	"15/10"
1.6		30	44
2.0	50	21	24
2.5	34	16	24
3.0	25	12	18
4.0	16	8	12
5.0	12	6	9
6	9	4	6
Note:	a is the distance from the measuring grid to the disturbance, D_h is the hydraulic diameter of the channel, tube, tunnel,..		

The EN 12599 also gives a formula to calculate the uncertainty of the measurements after measurements are done. This does not only take in account the influence of large obstacles, but also those (small) obstacles that were overseen and the roughness of the walls. Thus, it is best to first use the rule of thumb to determine the distance from large obstacles and with the amount of measuring points used. The rule of thumb will give a rough idea if the position is the most favourable position for the most accurate measurements. Afterwards it is possible to calculate the relative uncertainty with following formula[1] for the irregularity of the velocity profile and Table 2.4:

$$U = \frac{v_{max} - v_{min}}{2\bar{v}} \tag{2.2}$$

With:

U:	irregularity of the velocity profile
$\bar{v}$:	mean(arithmetic) velocity $[m/s]$
v_{max}:	maximum mean velocity of all quadrants
v_{min}:	minimum mean velocity of all quadrants

Once the irregularity of the velocity profile is determined, the relative uncertainty of the measuring location τ_u can be calculated. Table 2.4 gives an example of of the change in accuracy depending on the amount of measuring points and the irregularity U of the velocity profile.

[1]Note: this formula is adopted by the EN 12599 in case all the velocities of the different probes are used to calculate one average value for further use in network models. However, this will also be applied for the 2D analysis in this dissertation since the obstacles considered with this formula are the ones that were overseen when determining the location for the measuring grid.

Table 2.4: Relative uncertainty in function of irregularity of U and the number of measuring points

Number of measuring points n	Relative uncertainty of the measuring location τ_u [%]					
	Irregularity of the velocity profile U [%]					
	2	10	20	30	40	50
25	2	4	7	10	13	16
36	1	3	6	8	11	13
49	1	3	5	7	9	11
Note:	this Table follows the formula: $\tau_u = 2.314 * U * n^{-0.552} - 0.895 * U * n^{-0.698} + 13.725 * n^{-0.778}$					

2.4 Uncertainties in the dissertation

The tests will be executed with a fixed frame and a digital read out of the results, thus guaranteeing the repeatability of the tests. Tests will be done over a period of 180 seconds, with a digital read out every second. The systematic error and the uncertainty coming with it will be neglected since there is lacking data to determine the uncertainty of the robustness of the frame. The robustness of the frame is defined as the resistance against the velocity passing by the frame, resulting in a force on the frame. Since the frame is braced and provided with a wind bracing the effects of the wind will be neglected.

Uncertainties that are taken in account are the uncertainty of the probes and the uncertainty whether the velocity profile is uniform or not [2]. Those are the two uncertainties that will have the strongest effect on the values of the measurement results. It is assumed that the vibration of the probes due to the wind passing by at sometimes high velocities is taken into account in the uncertainties given by the manufacturer after doing the calibration tests. The probes are fixed to the frame.

The hot ball probes were calibrated according to DIN EN ISO 9001:2008 and said to have a tolerance level of $\pm(0.03m/s \pm 5\%$ of the velocity value).

[2]Valid for a zone where a constant velocity profile is expected, when measuring close to the boosters to determine this uncertainty factor will not be taken into account

Chapter 3

FFMVisualizer (Flow Field Measurement Visualizer) - Software for more efficient data processing

In order to have an efficient post processing routine, a software was written during this thesis in Python. The program imports the velocity and pressure measurements as an .csv-files to compute the Volume Flow Rate and the Wall Roughness (the calculations based on the pressure drop over a length L can be found in Chapter 4.9.4). Additionally the program calculates the Density and the Hydraulic Diameter based on input parameters defined by the user when starting the program. The feature of plotting the slice file at the position of the measurement is also included. The end result can be seen in Figure 3.1. The code can be found in Annex C.

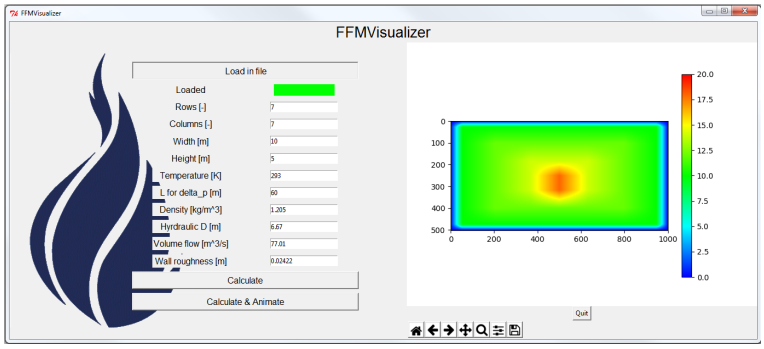

Figure 3.1: Screen shot of the GUI of FFMVisualizer

3.1 Input

For the program to be able to calculate everything, the following inputs are necessary:

- .csv-file of the velocity and pressure measurements of the entire grid per measuring location

- Number of rows and columns of the grid used to measure
- Width of the cross section $[m]$
- Height of the cross section $[m]$
- Temperature at the moment of measurement $[K]$
- Length of the tube used for the pressure measurements $[m]$

In order to have an efficient data processing, it is necessary to not have to close the program every time to load in a new file, cross section or grid. Therefore the main body was written as a 'self' function. In this way it is possible to alter all the inputs without having to close and restart the program.The 'self' function enables to overwrite the existing values. When the calculate-button is hit, the program takes the changed values and executes the integrated formulas and plot.

3.1.1 .csv-file

A .csv-file is being read in by the program. The Volume flow and Wall Roughness calculations are based on this file. For every measurement a separate .csv-file will be produced. The .csv-file has to be set up manually, the necessary data is collected from the output excel files from the data loggers (TESTO 480). Those excel files contain excessive information and can only show the data of the probes connected to the data logger.

The .csv-file that will be the source for the calculations and is an empty excel file with pre-numbered columns, see Figure 3.2. Each column corresponds to a location of the measuring grid and the corresponding data will be pasted in that specific column.

	A	B	C	D	E	F	G	H	I	J	K
1	1.1	1.2	1.3	1.4	1.5	1.6	1.7	2.1	2.2	2.3	2.4
2											
3											
4											
5											
6											
7											
8											
9											
10											

Figure 3.2: Screenshot of the .csv-file

For the CFD part of the thesis an Excel-file with the same name is made. This file has two worksheets. The first worksheet will be equal to the one of the .csv-file. The second worksheet will show the matrix with the average velocities, as well the average pressure and velocity of the measurements for determining the wall roughness. The matrix of average values will then be compared with a similar matrix produced from the simulation results.

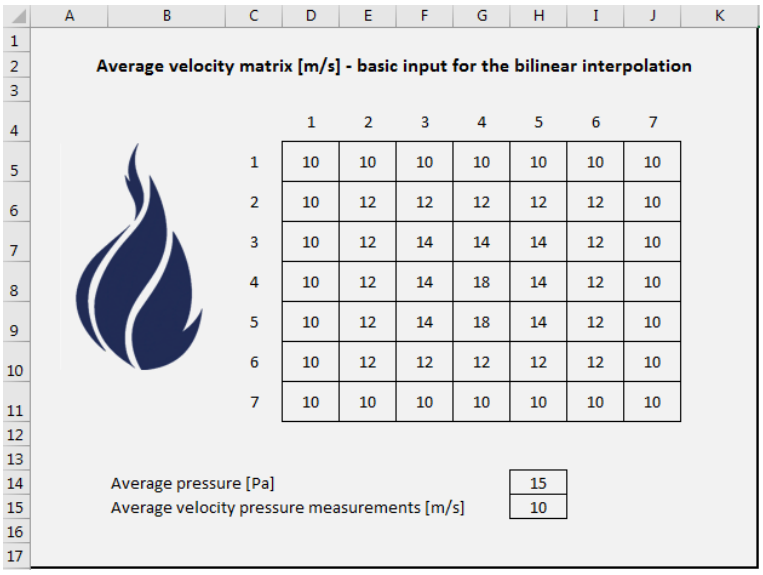

Average velocity matrix [m/s] - basic input for the bilinear interpolation

	1	2	3	4	5	6	7
1	10	10	10	10	10	10	10
2	10	12	12	12	12	12	10
3	10	12	14	14	14	12	10
4	10	12	14	18	14	12	10
5	10	12	14	18	14	12	10
6	10	12	12	12	12	12	10
7	10	10	10	10	10	10	10

Average pressure [Pa]	15
Average velocity pressure measurements [m/s]	10

Figure 3.3: Screenshot of the second worksheet of the Excel-file, filled in with example values

3.2 Output

The program gives two type of outputs: a slice file and a couple of numbers. Those numbers are:

- Density $[kg/m^3]$
- Hydraulic Diameter $[m]$
- Volume flow rate $[m^3/s]$
- Wall roughness $[m]$

The slice file is a plot of a 1000x1000 matrix based on the input matrix from the .csv-file, generated through bilinear interpolation.

As a check to see if the file is loaded, a box is added next to the text "loaded" which turns green when a file is loaded correctly.

3.3 Illustrative example

For a dataset of a 5x5 grid at position 15.4m where the width is 5.3m, the height is 9.2m, the measured temperature was 9.5°C = 282.65K) and the pressure was measured over a length of 60m, a screen shot was taken from the software.

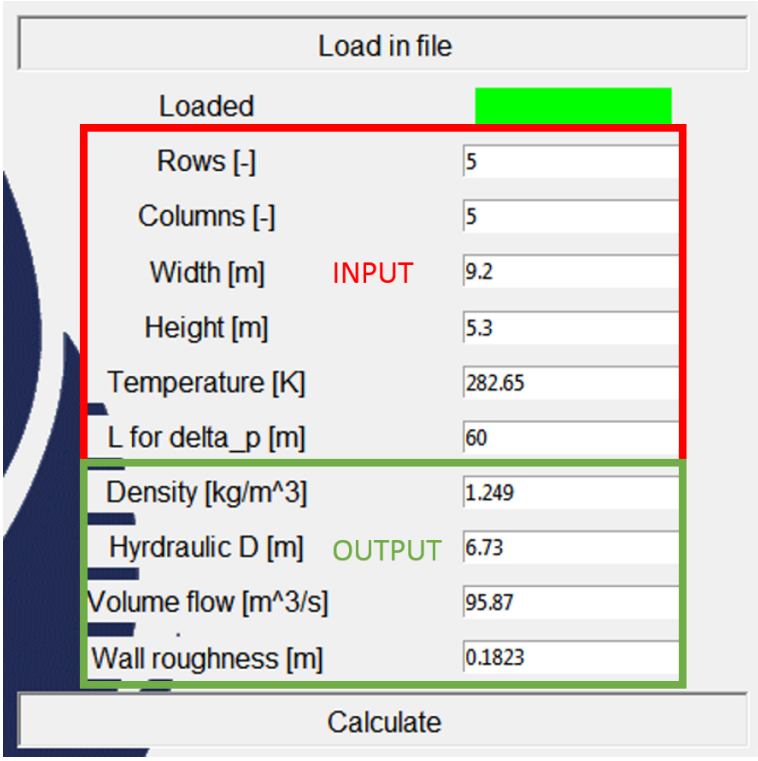

Figure 3.4

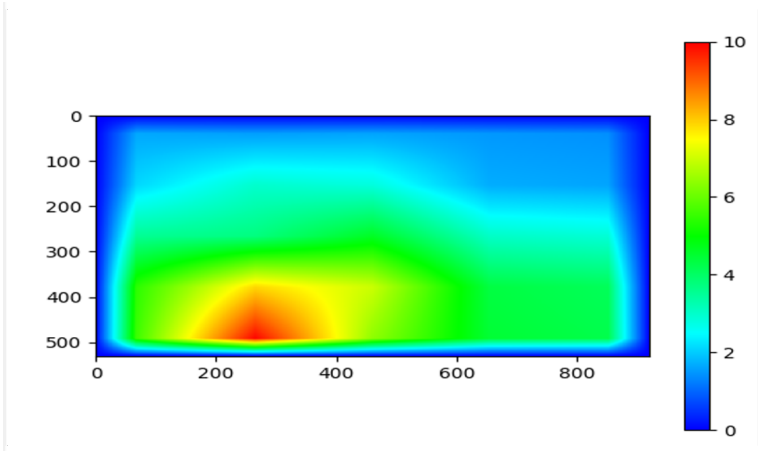

Figure 3.5: Plot of the averaged velocity profile, scale in m/s

Chapter 4

Experiment 1: Mobile fan in the Jan De Vos Tunnel

4.1 Location

After conversation with Agentschap Wegen & Verkeer, the Jan De Vos tunnel was reserved for the tests.

The Jan De Vos tunnel is located in the South-South-West of the city of Antwerp, and ensures a connection with the traffic junction Antwerp-Centrum and the A12 towards Brussels.

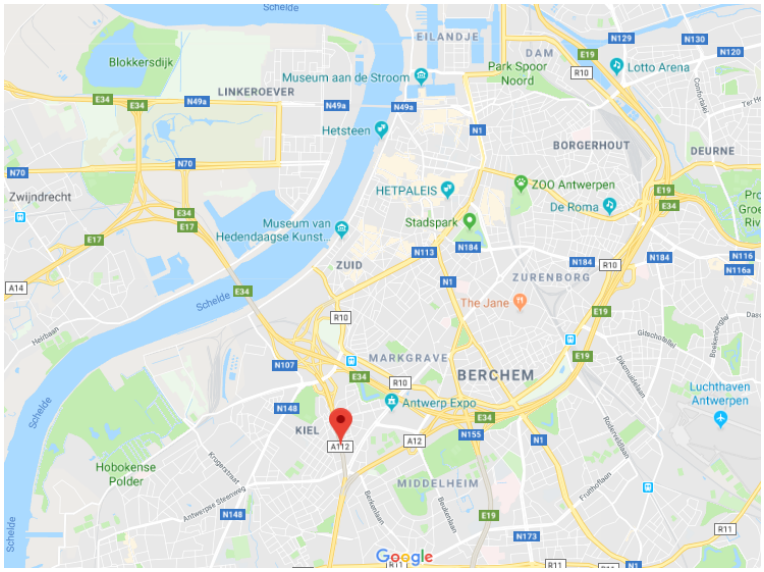

Figure 4.1: Map city of Antwerp with a mark for the Jan De Vostunnel

4.2 Geometry

The tunnel has two driving lanes and one pedestrian path meant for evacuation as can be seen in figure 4.2. The height at the measuring locations (under a beam of 75cm, total height = 6.05m, see also Figure 4.26) is 5.3m and the total width is 9.2m. The two driving lanes are 8m wide in total.

Figure 4.2: Geometry Jan De Vos Tunnel

4.3 Measuring equipment

For the purpose of this dissertation, the 18 hot bulb probes + measuring devices (testo 480) of FESG were used. The probes are from the brand Testo. The technical papers are given in Annex B. The hot bulb probes have an accuracy of ± (0.03 m/s ± 5% of the velocity value). The total relative uncertainty of the experiment will be discussed in sub chapter 4.9.

Figure 4.3: Hotbulb probe (left) and Testo 480 (right)

4.4 Measuring grid

The measuring grid is built as is considered in the ISO 5802 code and as explained in chapter 2. For this experiment, three different grids are used to determine the difference in accuracy of each measuring grid, going from 25 points (coarse) to 49 points (fine). Figures 4.4 - 4.6 show the measuring grid with the relevant distances for the experiment in situ.

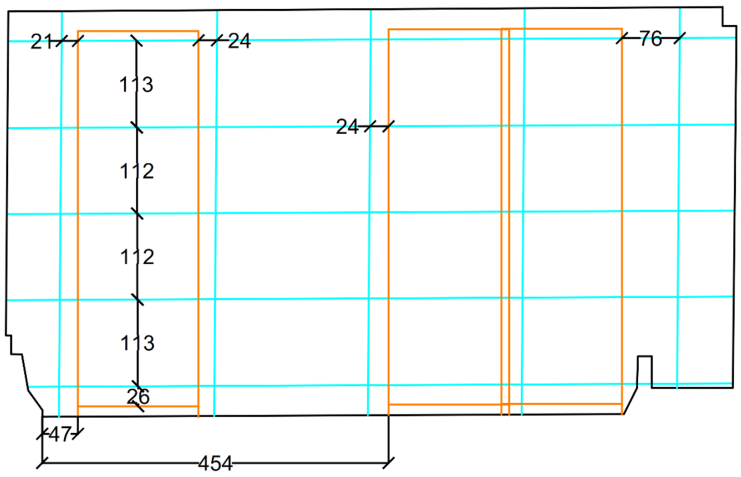

Figure 4.4: Measuring grid with 25 points

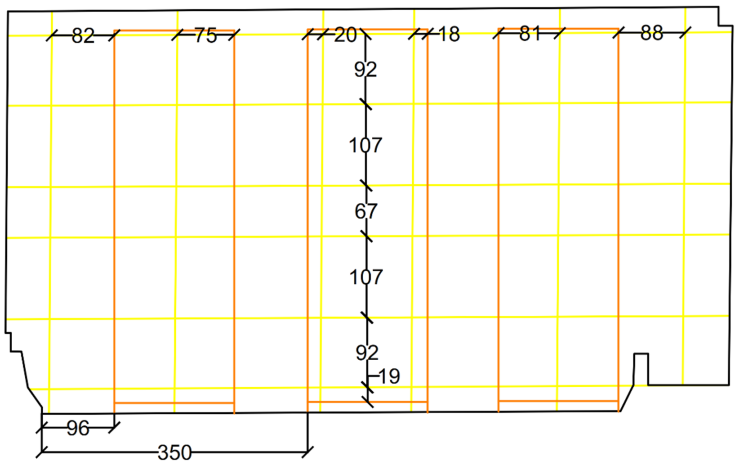

Figure 4.5: Measuring grid with 36 points

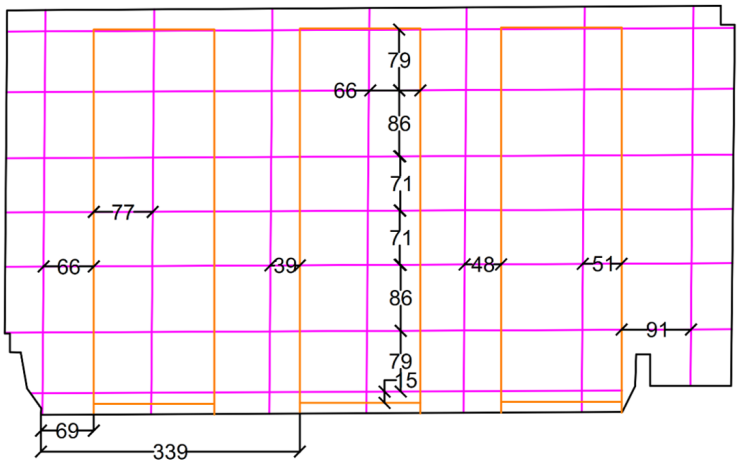

Figure 4.6: Measuring grid with 49 points

4.5 The Frame

Aluminium profiles form the basis of the frame. The reason for choosing this type of profile for the build-up of the frame is that three different grids are measured, and these profiles permit the flexibility necessary for doing so. The aluminium profiles are attached to each other with a system as shown in Figure 4.7. The rectangular nut is inserted in the channel and the outer shell of the bolt is fixed in the channel at the end of the profile. To connect the two profiles, the bolt is pushed through the shell and afterwards fixed in the rectangular nut. The probes are attached to the frame with triangles as shown in Figure 4.8, the triangles are fixed with the rectangular nuts. All together the frame is as in figure 4.9.

Figure 4.7: Connection bolt

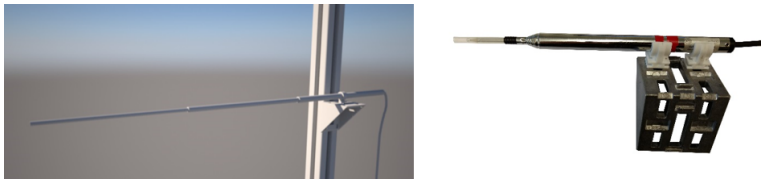

Figure 4.8: 3D design connection probes to frame + actual connection

Figure 4.9: Aluminium frame

4.6 Characteristics of the mobile fan unit and its expected performance according to the theory

The Fire Brigade Zone Rand has a BIG MGV L105 type of mobile fan with the following theoretical characteristics:

Table 4.1: Characteristics of mobile fan unit

Outlet volume flow $[m^3/h]$	145,000
Outlet velocity $[m/s]$	50
Power consumption $[kW]$	55
Angle of cone $[degrees]$	NP
A_c $[m^2]$	0.78

With formulas given by Woods [10] and Shan K. Wang [11], the maximum centreline velocity and throw length can be calculated. These formulas are for a free isothermal jet, in a tunnel the jet will be constrained. The values in practice have a high chance of being higher. As soon as the jet reaches the boundaries of the tunnel, the formulas can not be applied any longer. This can be also explained when looking at the mass balance in the tunnel, from the point the jet reaches the boundaries, no extra mass can come in and no mass goes out. The following formulas give an idea on how the fan will perform in the first couple of meters until the jet reaches the boundaries and how it would perform in free air.

- Maximum centreline velocity at x [11]:

$$V_x = \frac{K' v_f \sqrt{A_0}}{x} \tag{4.1}$$

With:

V_x: Maximum centreline velocity $[m/s]$
$K^{'}$: constant, $K^{'} = 1.13K = 7$, $K = 6.2$ for round openings with an outlet velocity between 10 and 25m/s
v_f: outlet velocity $[m/s]$
A_0: $A_c C_d R_{fa}$, R_{fa} is the ratio of the free area over the gross area of the outlet $[m^2]$
$R_{fa} = 0.95$, this is an assumption since there are 5 guide vanes with limited surface area.
C_d: discharge coefficient = 0.9

For this case:

Table 4.2: V_x for different values of x

$x[m]$	$V_x[m/s]$
15.4	18
27	11
38.4	7
50	6
61.4	5

- Throw length of the fan (in free air), the distance from the fan where the centreline velocity is equal to 0.5 m/s[11]:

$$X_t = \frac{K^{'} Q_0}{V_x \sqrt{A_0}} \tag{4.2}$$

With:

X_t:	Throw length $[m]$
V_x:	centreline velocity equal to 0.5 m/s
Q_0:	Supply volume flow rate $[m^3/s]$

For this case: $X_t = \frac{7*29.20}{0.5*\sqrt{0.78*0.95*0.9}} = 501m$

- Angle of the cone: not provided.

4.7 Test procedure

4.7.1 Visual inspection

Before proceeding with the experiment a visual inspection should be done in order to have an accurate CFD simulation. This visual inspection should highlight obstacles, open doors, emergency exits nearby, water, etc...

4.7.2 Placing the mobile fan

The mobile fan is planted 30m in the tunnel as would be the case in a real life situation when a car fire is occurring in the tunnel.

Figure 4.10

4.7.3 Placing the grid

The grid is located on different distances from the mobile fan: a, 15.4m, 27m, 38.4m, 50m and 61,4m. The frame placed at distance a from the mobile fan is such that the influence of obstacles or turbulence caused by the fan is assumed to be of no great disturbance for correct measurements, a/D_h is taken according to EN 12599, see Table 2.3. To have the least disturbance and thus the highest accuracy, a factor of 6 is chosen. With a hydraulic diameter D_h=6.59m, a is then equal to 39.54m. The five extra positions will be under a beam that is present every 11.50m, starting from point 34m (distance to the portal, not the fan). The cross-section at 39.54m from the fan shows a non-uniform ceiling (see Figure 4.13), this makes it impossible to measure the velocity profile correctly with the grids being used. Since a measurement will also be performed at 50m from the fan, there is no need to provide for an extra measuring location to cover the distance a determined by using the code EN12599.

In order to have the right measurements, the measured values will be normalised with reference probes placed 20m before the fan. For every test location, the first measured value of the reference probe will define the denominator for the normalisation of the measured data from the reference probe. The normalisation will permit to estimate the influence of the wind and to adapt measured data where necessary. The normalisation is necessary because the frame will be moved horizontally for every test location to map the entire flow field.

For the pressure measurements a grid of 14 probes will be placed at a position in the tunnel where it is expected to have a constant pressure drop per meter over length L=60m.The requirement of having a constant pressure drop is such to be able to utilize formulas that use the assumption of an environment with no large turbulence fluctuations. See also Figure 4.11 and 4.12.

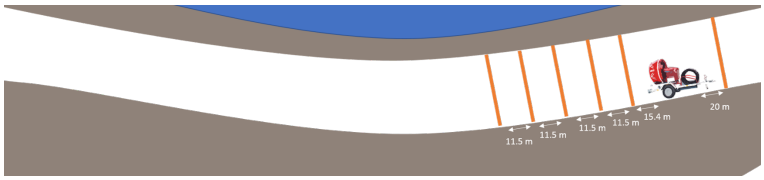

Figure 4.11: Positioning of the frame in Jan De Vostunnel - velocity measurements

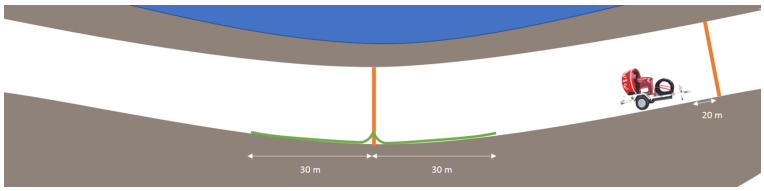

Figure 4.12: Positioning of the frame in Jan De Vostunnel - pressure measurements

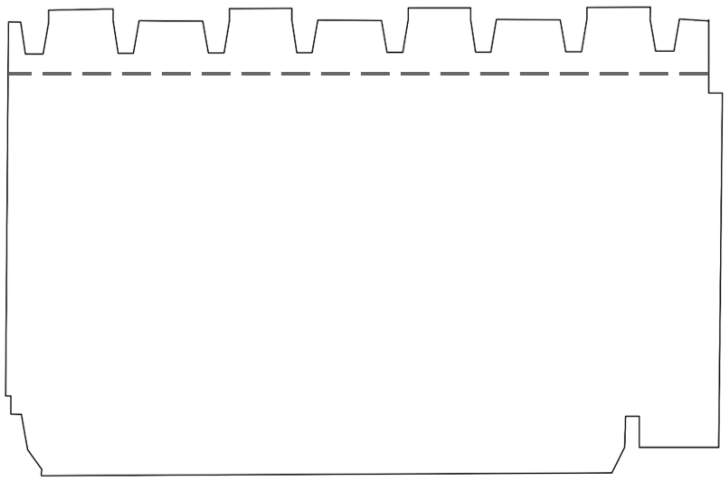

Figure 4.13: Cross-section at position a, the dotted line represents the bottom of the beams

4.7.4 Perform the test

As mentioned before, prior to the start of the experiment a visual inspection should be done. The frame is positioned on 5 different positions in the tunnel. Three different grids are used: 25 (5x5), 36 (6x6) and 49 (7x7) points. Since FESG has 18 probes, the frame has to be moved horizontally to cover the entire grid. The use of reference probes makes it possible to measure in this way. A separate measurement is done in order to calculate the friction coefficient Rf of the tunnel. Both pressure and velocity will be measured. A total of 50 measurements of 180 seconds each are done. An overview can be seen in Table 4.3.

Table 4.3: Overview tests for Experiment 1

	Test number		
	25 points	36 points	49 points
45.4m	1-3	16-18	32-35
57m	4-6	19-21	35-38
68.4m	7-9	22-24	39-42
80m	10-12	25-27	42-45
91.4m	13-15	29-31	46-49

4.8 CFD Simulations

After the flow field measurements, results from CFD simulations using FDS 6.5.3[12][13] are compared with the measured data and afterwards the boundary conditions of the simulations will be adapted to have a better match with the measured data.

4.8.1 Design of the mobile fan

In order to be able to model the mobile fan in FDS, it is important to know the mesh size used in the simulation. Because the fan will generate zones of high turbulence in and around the jet of the fan, a sensitivity analysis is necessary,

4.8.1.1 Sensitivity Analysis

Three cases were set up for a fan measuring 0.8m by 0.8m and a tunnel with a length of 100m with the same width and height of the Jan De VosTunnel. The first mesh had cells of 0.4mx0.4mx0.4m (REK_02_0), the second had cells of 0.2mx0.2mx0.2m(REK_03_0) and the third was 0.1mx0.1mx0.1m (REK_04_0).

The mean velocity and the volume flow rate at the portals of the tunnel, the pressure profile in the tunnel and the length and shape of the jet were considered for the sensitivity analysis. Figure 4.14 to Figure 4.16 represent the comparison of the three different meshes for the

pressure profile, the pressure differential, the mean velocity at the portals of the tunnel and the volume flow rate at the portals of the tunnel. Figure 4.17 displays the visual comparison of the jet between the three different grids. As can be seen, the mean velocity at the entrance, the pressure profile and the pressure differential show no distinct difference between the three different meshes. The difference is demonstrated in Figure 4.17, the white lines mark the points of comparison. The shape of the jet just after the fan can already demonstrate that a mesh with cells of 0.4mx0.4mx0.4m is not fine enough to model the fan. From the slice file one could think that the the lower part of the fan is modelled to induce a velocity that is slower than the upper part. Without comparing with the other simulations, it can be said that this is not correct. A cell size of 0.4mx0.4mx0.4m will not be used to model the fan and the region around the fan. Out of the two remaining simulations it is hard to say that a distinct difference is present. The jet has a similar shape and length for both meshes. It can thus be concluded that a mesh with cell size of 0.2mx0.2mx0.2m will be used to model the fan.

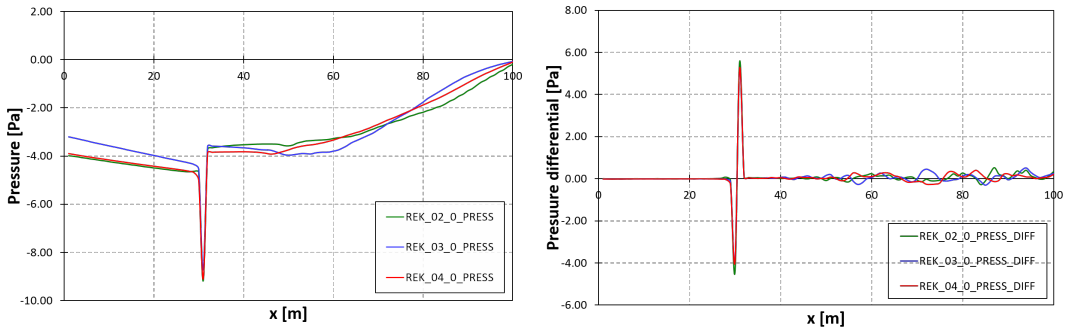

Figure 4.14: Sensitivity analysis, Left: Pressure $[Pa]$; Right: Pressure differential $[Pa]$

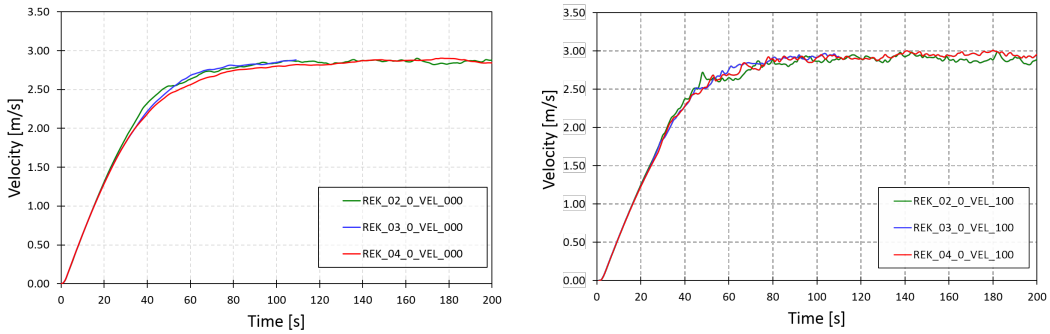

Figure 4.15: Sensitivity analysis, Left: Velocity at 0m $[m/s]$; Right: Velocity at 100m $[m/s]$

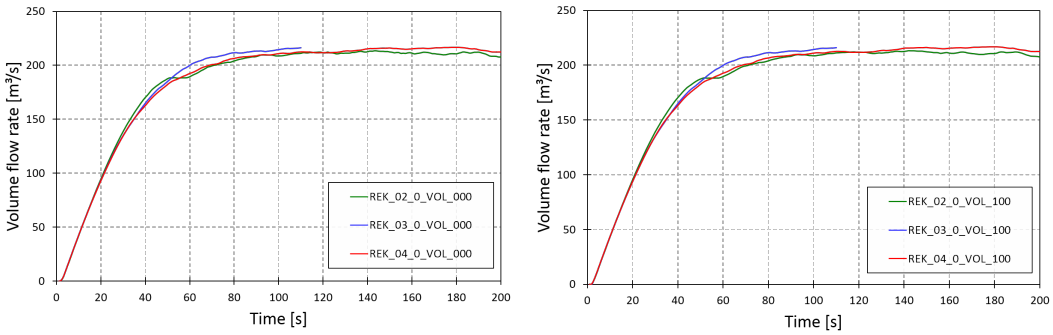

Figure 4.16: Sensitivity analysis, Left: Volume Flow Rate at 0m $[m^3/s]$; Right: Volume Flow Rate at 100m $[m^3/s]$

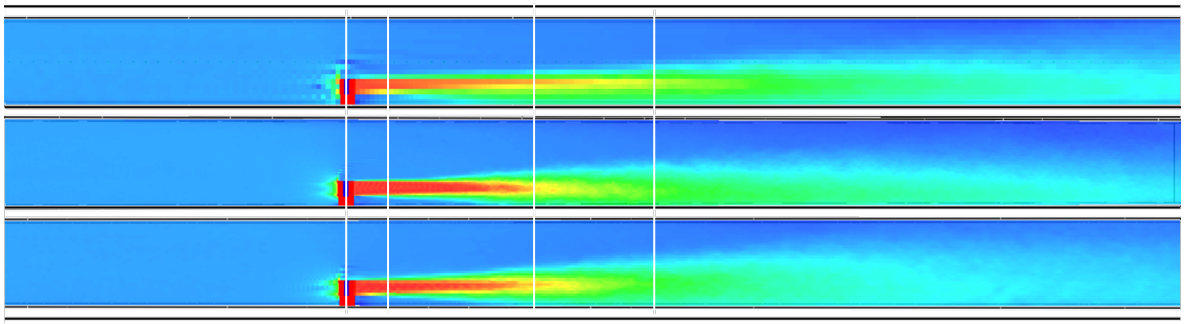

Figure 4.17: Sensitivity analysis (maximum velocity is 20.5m/s): first image is 0.4mx0.4mx0.4m, the second is 0.2mx0.2mx0.2m and the third is 0.1mx0.1mx0.1m

4.8.1.2 Design

Considering the sensitivity analysis demonstrated that a grid of 0.2mx02x0.2m is sufficient for this research, the fan was modelled as a series of cubes with size 0.2mx0.2mx0.2m (see also Figure 4.18.) Because the modelling was done after the tests, three different zones can be seen in Figure 4.18: a zone where the velocity is $36.5m/s$ (average measured value, with peaks of $40m/s$), a zone with $26m/s$ and a zone that has almost no velocity due to the engine placed behind the fan.

The inlet and the outlet of the fan were modelled as 14 vents, 7 for the inlet and 7 for the outlet. The total surface of te inlet/outlet of the fan equals $0.8m^2$, the difference in surface between the modelled fan and the real fan is $0.02m^2$. An obstacle was created between the inlet and the outlet of the fan with a thickness of 0.2m. The inlet and outlet where connected with a duct having default values (&HVAC ID='Duct_8', TYPE_ID='DUCT', DIAMETER=0.451352, FAN_ID='FAN_1', NODE_ID='Node_8_01','Node_8_02', ROUGHNESS=1.0E-3/). For every 'FAN' linked to one of the 7 vents, the volume flow rate was calculated respectively to the surface of the vents.

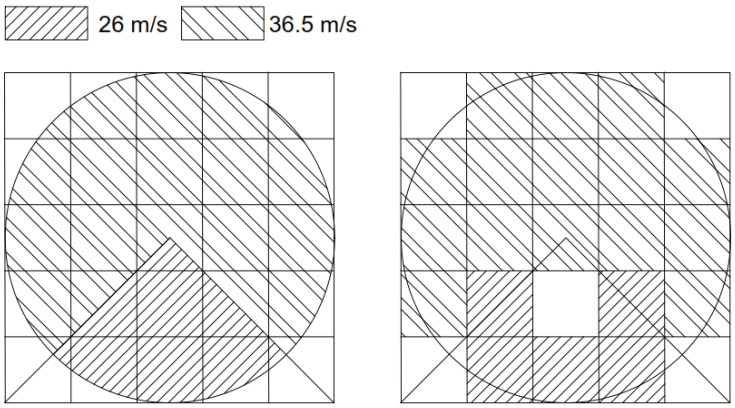

Figure 4.18: Sketch of the modelling of the fan, each cell is 0.2mx0.2m. Left: real surface fan, Right: FDS surface fan

4.8.2 Design of the tunnel

For the most accurate results, a contour was drawn in AutoCad on the image from the tunnel cross-section and afterwards the .dxf-file was imported in GoogleSketchup to extrude the shape of the tunnel. This option was chosen due to the complex geometry of the tunnel. After modelling a part of the tunnel in GoogleSketchup, the 3D-model was exported as a .dxf-file and in Pyrosim. The tunnel walls, ceiling and floor were defined as an 'INERT' material. The imported 3D-model has excessive faces. Those were carefully deleted and where necessary replaced with obstacles. After a preliminary run with a mesh with cell size 0.2mx0.2mx0.2m, it was decided to work with different meshes for the portals, the first part of the tunnel (0m-112m) and the second part of the tunnel (112m-740m). This was done to reduce the calculation time of the simulation. The meshes of the portals and the second part of the tunnel have a cell size of 0.4mx0.4mx0.4m, the mesh of the first part of the tunnel has a cell size of 0.2mx0.2mx0.2m. This is possible because the sensitivity analysis demonstrated that the velocity and the pressure distribution along the tunnel show no big difference when using a coarser mesh. The finer mesh is necessary because this is in an expected high turbulent region.

4.9 Results

4.9.1 Visual inspection + course of the tests

The visual inspection highlighted the presence of jet fans mounted on one side of the tunnel close to the ceiling. It also highlighted the lighting fixtures in the middle of the tunnel, which lowered the height of that part of the tunnel by roughly 60 cm. The presence of the jet fans had no influence for the placement of the frame, but the lighting fixtures did.

Because of the lighting fixtures being lower than the ceiling, indicated on the plan, the frame built did not fit underneath those fixtures. The frame tilting proved to be not possible after

multiple attempts. Since the tunnel is close to a rectangle, the assumption was made that with one half of the tunnel measured, the other half could be deduced through mirroring the data over the centre axis.

At the end of the originally planned experiments, five other unplanned measurements were set to investigate the influence of the horizontal position and the angle of the fan with the horizon. The frame was set at the same location as the pressure measurement. The five extra measurements were:

- fan in middle of the tunnel, angle = +25°
- fan in the middle of the tunnel, angle = -20°
- fan on the left[1] side of the tunnel, angle = 0°
- fan on the left side of the tunnel, angle = +25°
- fan on the left side of the tunnel, angle = -20°

From those few tests, it could be concluded that the most preferable conditions are those were the fan is in the middle with an angle of 0° with the horizon. If this is not possible, a set-up with the fan on the left side and an angle of -20° is the next preferable solution. Note that these conclusions are tunnel specific and may not be true for a tunnel with a different geometry, e.g. the type of ceiling (in this experiment a big contributor to the flow pattern of the flow induced by the mobile fan).

4.9.2 Characteristics of the mobile fan unit and its measured performance

There is often a big difference between the theoretical performance of a fan and the in situ performance of the fan. As already explained in the section 4.8, the velocity from the fan is not equal for every zone. This will result in a lower performance than what was provided by the manufacturer. In the following Table the characteristics in situ are given:

Table 4.4: Measured characteristics of the mobile fan unit

Outlet volume flow $[m^3/h]$	95472
Average outlet velocity $[m/s]$	34
Angle of cone $[degrees]$	7.4
A_c $[m^2]$	0.78

4.9.3 Post processing for the fire brigade of Antwerpen Rand

Given that the condition of road tunnels in Belgium that are already long in use can be poor, additional risks can emerge in case of fire. Hence, it is certainly useful to perform flow field measurements to investigate in which situation the mobile fan can improve the risk-level and provide sufficient safety for people present in the incident tunnel. To express the practical

[1] left side = side with no evacuation path

use of such mobile fans, a feasibility study was performed indicating in which situations the mobile fans prove to be an added value.

4.9.3.1 Data Flow Field Measurements

Due to the geometrical obstacles in the tunnel and time delay during the setting up of the tests, it was only possible to give a general view of the velocity profile with the 5x5 grid. As mentioned before, the assumption was made that measuring half of the tunnel, the data could be mirrored. In this way the complete flow field would be mapped. When post processing the data, it became clear that a mistake had been made during the tests of placing the fan in the middle of the road and not in the middle of the tunnel. For this very reason the data could not be mirrored. The Tables below show the average value for every probe on every location measured during the experiment.

Table 4.5: Average value for every probe of the 5x5 grid

(a) 15.4m

probe	1	2	3	4	5
1	0.79	1.09	0.87	-	-
2	1.08	3.24	1.87	-	-
3	1.41	4.45	4.76	-	-
4	2.15	8.55	7.18	-	-
5	4.01	12.57	7.09	-	-

(b) 27m

probe	1	2	3	4	5
1	1.66	1.57	1.62	-	-
2	2.14	2.98	2.82	-	-
3	3.54	3.74	4.63	-	-
4	5.43	7.87	6.99	-	-
5	5.60	9.94	6.42	-	-

(c) 38.4m

probe	1	2	3	4	5
1	1.54	1.28	1.53	-	-
2	2.57	2.36	2.68	-	-
3	3.86	2.90	4.20	-	-
4	5.26	5.68	5.45	-	-
5	5.12	6.63	5.41	-	-

(d) 50m

probe	1	2	3	4	5
1	1.90	1.61	1.54	-	-
2	2.77	2.72	2.61	-	-
3	3.54	2.66	3.54	-	-
4	4.24	4.39	3.59	-	-
5	3.64	4.34	4.24	-	-

(e) 61.4m

probe	1	2	3	4	5
1	2.25	1.95	1.62	-	-
2	2.57	2.75	2.77	-	-
3	2.93	2.45	3.27	-	-
4	3.29	3.44	2.68	-	-
5	3.03	3.14	3.65	-	-

The flow field measurements show that the distance from the fan, to a point where the velocity profile is almost fully developed, is past 61m. Even with the incomplete data set, it is possible to say that a fully developed velocity profile will exist behind 61m. Assume this length to be

another 23m further, so in total 84m or 13 hydraulic diameters. Note, this length is dependent on the geometry of the tunnel and the position of the fan. The recommendation made to the fire brigade was to take into account at least a length of 61m or 10 hydraulic diameters for tunnels similar in geometry to that of the Jan De Vostunnel, to reach an almost fully developed velocity profile.

The average velocity of the almost fully developed velocity profile at 61m from the fan, is roughly 2.7m/s. This is in cold conditions with an average temperature of $9.5°C$ en without large wind influences. In case of fire, the pressure losses will increase, both the local pressure loss due to the fire and the linear losses downstream. Because of these phenomena, the fan will have to deliver more power to maintain the same velocity of the air before the fire. The fan was running at full capacity during the experiment and thus when using this fan for an intervention, the fire brigade will have to take into account that the generated velocities will be less than what was measured in cold conditions.

4.9.3.2 Data Pressure Measurements

The pressure measurements were executed at 120m from the fan to be able to guarantee a regime with no large fluctuations. This is important to be able do the calculations for the wall roughness with formulas used in this thesis. As explained earlier, the pressure drop was measured over a length of L=60m. The data from these measurements is very limited and is written down in Table 4.6. The values displayed are an average over 180 seconds of measurement. The calculations of the wall roughness will be discussed in sub chapter 4.9.4.

Table 4.6: Average value of the pressure measurements per device

Device	Pressure $[Pa]$
1	-1.5
2	-1.3

4.9.3.3 Calculation of the back-layering

In the previous chapter, the measured data were discussed and a note was made that the values from the measurements were an indication of how the fan performs in a cold environment and what the real volume flow rate and velocity were, as generated by the fan.

The strongest relevance of the tests for the fire brigade is to know in what incident situations the mobile fan can be put into action. For this it is important to calculate the critical velocity in the tunnel and the velocity generated by the fan in hot conditions. Nine cases are investigated to see how the fans would perform in different fires and situations. Three fires were chosen as a possible fire in a tunnel: a car fire (5MW), a bus fire (30MW) and a truck fire (100MW). Because the Fire Brigade of Antwerp has also recently bought two mobile fans (1 BIG MGV L105 and 1 BIG MGV L125), three set-ups where simulated: 1 x L105, 2 x

L105 and 1 x L105 + 1 x L125. The critical velocity, the induced velocity in the incident tunnel and the backlayering length were calculated for those nine different cases.

"If the ventilation velocity is low, the smoke produced from the fire can travel in the upstream direction against the direction of the ventilation air. This reversal of flow is called 'backlayering'. The 'critical velocity' is used to represent the value of the ventilation velocity which is just able to eliminate the backlayering, and force the smoke to move in the downstream direction. This value has become one of the prime criteria for the design of tunnel ventilation systems."[14] The calculations for the critical velocity were based on the formula's of Wu and Bakar[14] and Li and Ingason[4]. For the calculations of the backlayering length, the formulas of Li and Ignasson[4] were used.

"The governing parameters for the critical velocity in a longitudinally tunnel are the heat release rate, air density, ambient temperature, thermal capacity of air, gravitational acceleration, tunnel geometry and tunnel slope. The height of the tunnel is taken to be the characteristic length in the assumption that the ratios of width to height in tunnels are usually of the same order." [4] The critical velocity according to Li et al. can be expressed as[4] :

$$V_c = f(Q, \rho_0, c_p, T_{amb}, g, H) \tag{4.3}$$

The dimensionless critical velocity is expressed as [4]:

$$V_c^* = \frac{V_c}{\sqrt{gH}} = f\left(\frac{Q}{\rho_0 c_p T_{amb} g^{1/2} H^{5/2}}\right) = f(Q^*) \tag{4.4}$$

From the research of Li. et al. a piecewise function can be expressed as:

$$V_c^* = \begin{cases} 0.81Q^*, & Q^* \leq 0.15 \\ 0.43 & Q^* > 0.15 \end{cases} \tag{4.5}$$

The dimensionless critical velocity defined by Wu and Bakar [14] uses the same expression for the dimensionless HRR and the critical velocity and can be expressed as:

$$V_c^* = \begin{cases} 0.40(0.20)^{-1/3}(Q^*)^{1/3}, & Q^* \leq 0.20 \\ 0.40 & Q^* > 0.20 \end{cases} \tag{4.6}$$

Because for equations 4.3 to 4.6 the slope was assumed to be zero degrees, an extra formula by Atkinson and Wu[15] was drawn up and can be expressed as:

$$V_c^*(\theta) = V_c^*(0^\circ)(1 + 0.014\theta) \tag{4.7}$$

Both functions (Li and Wu and Bakar) are displayed in Figure 4.19

The governing parameters for the backlayering length are almost the same as for the critical velocity, the longitudinal ventilation velocity V was added, and can be expressed as:

$$L_{bl} = f(Q, V, rho - 0, c_p, T_{amb}, g, H) \tag{4.8}$$

The dimensionless backlayering length can be expressed as:

$$I^* = \frac{L_{bl}}{H} = f\left(Q^*, \frac{V^2}{gH}\right) = f(Q^*, V_c^*) \tag{4.9}$$

Li et al. developed a piecewise function, based on experimental data and an be expressed as:

$$I^* = \begin{cases} 18.5ln(0.81(Q^*)^{1/3}/V^*), & Q^* \leq 0.15 \\ 18.5ln(0.43/V^*) & Q^* > 0.15 \end{cases} \tag{4.10}$$

An example of the function for a 30MW fire in the Jan De Vostunnel can be found in Figure 4.19.

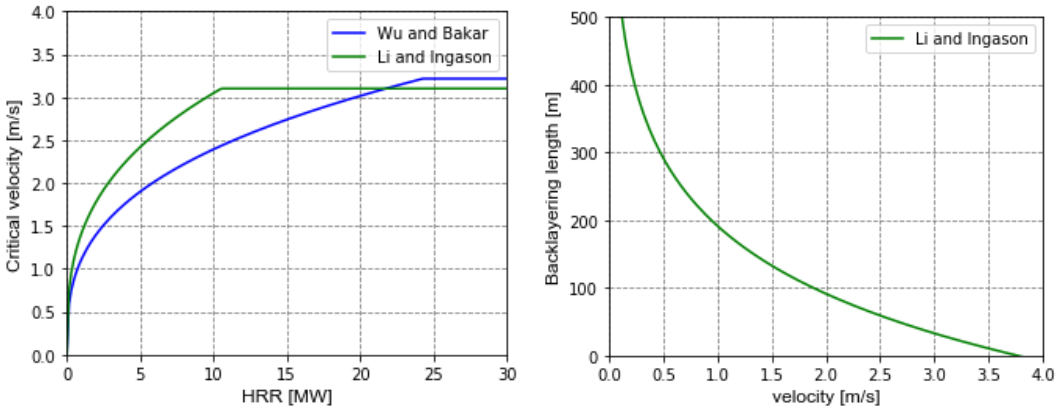

Figure 4.19: Left: critical velocity; Right: backlayering length for a 30MW using Li[4]

To perform the calculations it is also necessary to know the installation efficiency of the fan. The air stream induced by the fan is a jet that has the shape of a cone, the top corner of the cone can be in the range of 10° to 15°, dependent on the shape of the outlet. The energy of the jet is transferred to the surrounding air stream in the tunnel by means of friction at the surface of the cone. However, when the jet touches walls, ceilings, the road or components (lighting fixtures, speakers, signs, etc...) the energy is not entirely transferred to the air stream in the the tunnel. Because of this phenomenon a thrust loss is present, to take this into account when doing the calculations, an installation efficiency η_{inst} is introduced. [5] The installation efficiency is defined as:

$$\eta_{inst} = \frac{F_{f,eff}}{F_{f,real}} \cdot 100\% \tag{4.11}$$

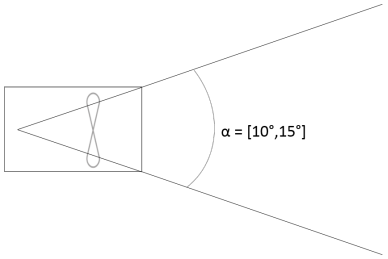

Figure 4.20: Sketch to illustrate the cone of a jet

The influence of the walls and ceilings on the installation efficiency of the fan is strongly determined by the distance from these elements to the fan. This efficiency was deduced from the graph given by the book "Aanbevelingen Ventilatie Van Verkeerstunnels" [5], see also Figure 4.21.

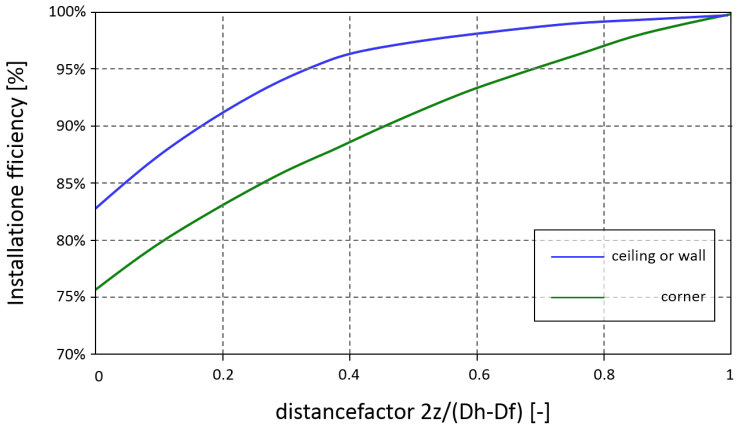

Figure 4.21: Installation efficiency dependence on the position of the fan, redrawn from [5]

$$distancefactor = \frac{2z}{D_h - D_f} \tag{4.12}$$

With:

z: Closest distance to a wall or ceiling [m]
D_h: Hydraulic diameter [m]
D_f: Inner free diameter of the fan [m]

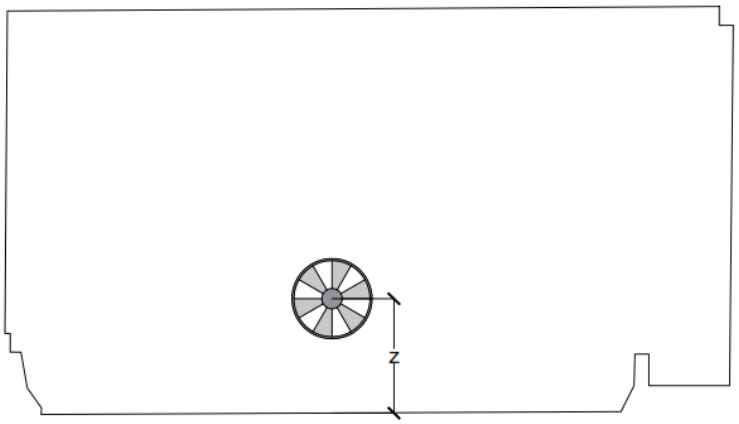

Figure 4.22: Position of the fan in the Jan De Vostunnel

For this case, $z = 1.5$m, $D_h = 6.59$m and $D_f = 1$m, thus Eq. 4.12 becomes: 0.54 and the installation efficiency equals 97%.

Other input parameters are the HRR, the position of the fire, the friction coefficient, the position of the fan, the free area of the fan and the outlet velocity. For the L105 it was measured to have an average outlet velocity of 34 m/s. With all the input parameters known, the nine cases could be computed. The friction coefficient was taken to be 0.024, which is 30% higher than what [5] recommends to use for rough walls and a normal road surface. The motivation for the higher friction coefficient were the frequently returning beams every 11.5m in the tunnel with a height of 75cm or 12% of the tunnel height. The calculations are done based on the momentum equation solved for steady state conditions along the whole tunnel, used for the single branch model (1D) by [16]:

$$\frac{1}{2}\int_0^{L_t}\left(f\frac{1}{D_h}dx+\sum\beta\right)\rho_0 v_t^2+\Delta P_{fan}+\Delta P_{fire}+\Delta P_{wind}+\Delta P_g=0 \tag{4.13}$$

The buoyancy force in the tunnel with slope α is modelled with the expression by Merci[17]

$$\Delta P_g=\int_0^{L_t}(\rho_0-\rho_{in})gsin(\alpha)dx \tag{4.14}$$

The pressure induced by the fan is calculated with a source change by Tarada [18]

$$\Delta P_{fan}=\frac{A_f}{A_t}\rho_0(v_f-v_t)v_f \tag{4.15}$$

With:

v_f: fan outlet velocity $[m/s]$
v_t: velocity in the tunnel $[m/s]$
A_t: area of the cross-section of the tunnel $[m^2]$

The wind pressure at the portals is expressed in equation 4.16, since the tests were done under calm wind conditions the velocity is taken to be 0 and thus will the wind pressure be equal to zero. Further explanation about the coefficient c_p used for the wind pressure can be found in [16].

$$P_{wind}=\frac{1}{2}\rho_0 v_{wind}^2 c_p \tag{4.16}$$

With:

v_{wind}: wind velocity $[m/s]$

Heat losses through the tunnel walls are not solved with the energy equation, but are modelled with a simplified approach proposed by Ingasson [19]. The temperature rise induced by the fire is equal to:

$$\Delta T_{fire}=\frac{2\dot{Q}}{3\dot{m}c_p} \tag{4.17}$$

With:

$\dot{Q}$: Heat release rate $[kW]$
$\dot{m}$: air mass flow rate $[kg/s]$

The temperature decay downstream the fire is expressed as:

$$T(x) = T_{amb} + \Delta T_{fire} exp\left(-\frac{hPx}{\dot{m}c_p}\right) \tag{4.18}$$

With:

h: lumped transfer coefficient $[kW/m^K]$
P: perimeter of the tunnel $[m]$

Because of the longitudinal section of the tunnel, there was a need to do the nine cases for both driving directions (2 tubes, one to Antwerp and one to Brussels).

The results are split into two parts, one part where the performance criterion is to have a higher velocity in the tunnel than the critical velocity, the other part is based on the performance criteria that a back-layering of 30m to 50m is allowed, these performance criteria where discussed in [16]. The results of the feasibility study are displayed below.

Looking at the first performance criterion, three cases are feasible. The second performance criterion provides for two extra cases to be feasible.

Table 4.7: Feasibility according to the first performance criterion - to Antwerp

	1 fan (1xL105)	2 fans (2xL105)	2 fans (L105 + L125)
5MW - auto	YES	YES	YES
30MW - bus	NO	NO	YES
100MW - Truck	NO	NO	NO

Table 4.8: Feasibility according to the first performance criterion - to Brussels

	1 fan (1xL105)	2 fans (2xL105)	2 fans (L105 + L125)
5MW - auto	YES	YES	YES
30MW - bus	NO	NO	YES
100MW - Truck	NO	NO	NO

Table 4.9: Back-layering [m] - to Antwerp

	1 fan (1xL105)	2 fans (2xL105)	2 fans (L105 + L125)
5MW - auto	-	-	-
30MW - bus	115	38	-
100MW - Truck	291	106	74

Table 4.10: Back-layering [m] - to Brussels

	1 fan (1xL105)	2 fans (2xL105)	2 fans (L105 + L125)
5MW - auto	-	-	-
30MW - bus	92	31	-
100MW - Truck	159	77	58

Table 4.11: Feasibility according to the second performance criterion - to Antwerp

	1 fan (1xL105)	2 fans (2xL105)	2 fans (L105 + L125)
5MW - auto	YES	YES	YES
30MW - bus	NO	YES	YES
100MW - Truck	NO	NO	NO

Table 4.12: Feasibility according to the second performance criterion - to Brussels

	1 fan (1xL105)	2 fans (2xL105)	2 fans (L105 + L125)
5MW - auto	YES	YES	YES
30MW - bus	NO	YES	YES
100MW - Truck	NO	NO	NO

4.9.3.4 Conclusions

After the Flow Field Measurements en post processing it can be concluded that with almost no wind influence and a fuel controlled fire[2], the L105 fan can be used in the Jan De Vostunnel for:

- An intervention with one car burning with an estimated HRR of 5MW.
- An intervention with two L105 fans and a fire of 30MW. The fire brigade will have to take into account that in this case a back-layering will exist with a length of roughly 40 m.
  - Note that this value was calculated under normal wind calm conditions and without obstacles (e.g. traffic jam).
  - Obstacles or the wrong set-up can cause the back-layering length to be larger than in perfect conditions, see 4.9.1.

[2]A fire with a HRR = 100MW is still fuel controlled in this case since the velocity in the tunnel never goes under 0.53 m/s. This is calculated with the assumption that one kg of air can be used to release 3MJ/kg. With $\rho = 1.249$ the equation $HRR = 3MJ/kg * \dot{m} = 3MJ/kg * \rho * v_t * A_t = 3 * 1.249 * v_t * 49.68$, when solved for v_t the minimum velocity in the tunnel has to be 0.53 m/s or greater to have a fuel controlled fire.

The use of multiple fans is preferable and is an option to be pursued in any case of fire in a tunnel. The deployment of the fans, whether parallel or in series, will depend on the conditions in the tunnel.

- For a tunnel such as the Jan De Vostunnel the advised deployment is to place the fans in parallel since the tunnel is short in length. For short tunnels the pressure losses are less important than gaining enough velocity to push the smoke back.
- For long tunnels it is advised to place the fans in series to handle the larger pressure losses due to the length of the tunnel.
  - The experiment showed that the distance from the fan to an almost fully developed velocity profile is 61m.
  - When placing the fan in series, the recommendation is to keep at least the 61m between the fans if possible to guarantee the maximum efficiency of both fans.

The deployment of such fans for large fires with a high HRR should always be pursued, but with taking into account that a substantial back-layering could exist and the with coming large heat fluxes.

For tunnels with an existing and working ventilation system dimensioned for a limited HRR, it can be interesting to deploy the mobile fans to improve the conditions.

A report, written in Dutch, can be found in Annex D.

4.9.4 Wall roughness calculation

The wall roughness was derived from the pressure drop [20] measurements done at a location where a constant decrease in pressure is expected. The pressure drop is then calculated by:

$$\Delta p = \frac{\rho f L v^2}{2 D_H} \tag{4.19}$$

With:

f:	friction coefficient [-]
L:	Length of the tube [m]
D_H:	Hydraulic diameter [m]

From equation (4.19) the friction coefficient can be calculated and the wall roughness can be derived from the Colebrook formula[11] [5].

$$\frac{1}{\sqrt{f}} = -2log\left(\frac{\varepsilon}{3.7 D_H} + \frac{2.51}{Re_D \sqrt{f}}\right) \tag{4.20}$$

With:

ε:	Wall roughness [m]
Re_D:	Reynolds number [-]

$$Re_D = \frac{\rho v D_H}{\mu} \tag{4.21}$$

With:

μ: Dynamic viscosity coefficient $[Pa \cdot s]$

Sutherland's equation [21] is used for the calculation of the dynamic viscosity:

$$\mu = \mu_0 \frac{T_0 + C}{T_{amb} + C} \left(\frac{T_{amb}}{T_0} \right)^{\frac{3}{2}} \tag{4.22}$$

With:

$\mu_0 = 18.27 * 10^{-6}$; $T_0 = 291.15K$; $C = 120K$

Table 4.13: Input parameters for equations (4.19) and (4.20)

L [m]	60.00
D_H [m]	6.59
Re_D (4.21)[-]	1039844
T_{amb} $[K]$	282.65
μ (4.22)$[Pa \cdot s]$	1.81 E-5

With all the input parameters calculated it is possible to solve equation 4.19 to the friction coefficient f. With f known, the wall roughness ε can be calculated. The wall roughness of the tunnel is with a $\Delta_p = -1.5Pa$ equal to 0.15m, this equals to a friction coefficient of 0.05.

When implementing the friction coefficient in Equation 4.13, with $\Delta P_g = 0$, $\Delta P_{wind} = 0$ and $\Delta P_{fire} = 0$, the tunnel velocity is equal to 2.18m/s. The measured velocity is 2.27 m/s. It is thus possible to say that it is correct to perform further calculations with a friction coefficient equal to 0.05.

4.9.4.1 New conclusion for 4.9.3.4

For the calculations with the 1D network model, the assumption was made that the friction coefficient was 0.024 due to the beams every 11.5m, which is already 30% larger than what [5] recommends to use for a tunnel with rough walls and a normal road surface. However, the wall roughness calculations showed afterwards that the friction coefficient of the Jan De Vostunnel is 0.05, this is 283% larger than what [5] recommends to use. Consequently the calculations were retaken and the Tables below show the new results for the 18 cases.

Although the feasibility study for the case of 1 L105 fan and a fire of 5MW shows that backlayering will occur over a distance of 7m, a CFD study should be performed to have the

exact backlayering. In this thesis it has been assumed that Li's formulas[4] are accurate for smaller fires (e.g 5MW).

The new results highlight the high importance of performing wall roughness calculations in advance of designing the ventilation system with a 1D model. Thus, it is important to stress that before a ventilation study is performed for a tunnel with a non-regular cross-section and/or with repeated large obstructions on the ceiling/walls, the wall roughness could accurately be determined using a mobile fan together with the necessary pressure measurements. In this manner the uncertainty of the wall roughness can be reduced and a more accurate design can be accomplished.

Table 4.14: Feasibility according to the first performance criterion - to Antwerp/Brussels

	1 fan (1xL105)	2 fans (2xL105)	2 fans (L105 + L125)
5MW - auto	NO/NO	YES/YES	YES/YES
30MW - bus	NO/NO	NO/NO	NO/NO
100MW - Truck	NO/NO	NO/NO	NO/NO

Table 4.15: Back-layering [m] - to Antwerp/Brussels

	1 fan (1xL105)	2 fans (2xL105)	2 fans (L105 + L125)
5MW - auto	7/3	-	-
30MW - bus	133/123	71/62	50/44
100MW - Truck	306/192	133/107	107/92

Table 4.16: Feasibility according to the second performance criterion - to Antwerp/Brussels

	1 fan (1xL105)	2 fans (2xL105)	2 fans (L105 + L125)
5MW - auto	YES/YES	YES/YES	YES/YES
30MW - bus	NO/NO	NO/NO	YES/YES
100MW - Truck	NO/NO	NO/NO	NO/NO

4.9.5 Visual comparison velocity profile between the different grid sizes using FFMVisualizer

Because of the above mentioned circumstances (see 4.9.1), the tests did not go as planned and not enough data was collected to perform a full comparison between the different grids. The lack of data do not make it impossible to check the influence of the cell size of the measuring grid. The probe locations were integrated in the simulation, on all the probe positions in the cross-section a 'VELOCITY'-device is present. This way the theoretical approach of the problem is still possible. Theoretically the outlet velocity of the fan and the volume flow rate do not need to be the same as the experiment since all the probes are measured in the same circumstances and at the same time.

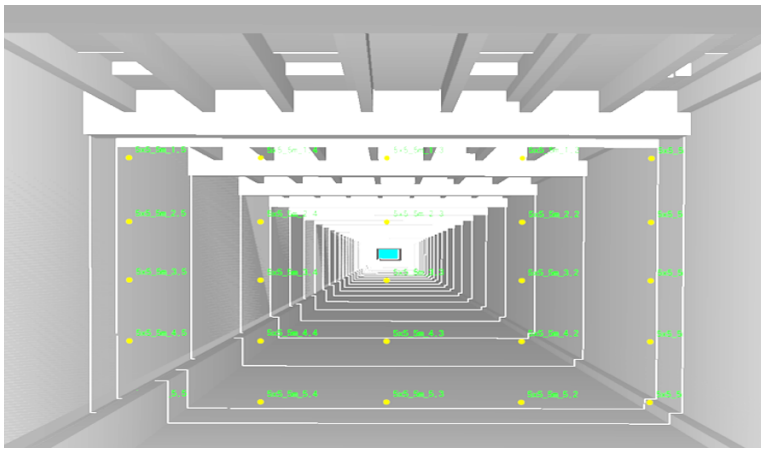

Figure 4.23: Screenshot out of Pyrosim - positioning of the probes in the cross-section for a 5x5 grid

The following picture is an overview of the slice files (generated with the use of FFMVisualizer) at the same locations as those from the flow field measurements based on the data recorded by the devices. The separate pictures for every slice file can be found in G.

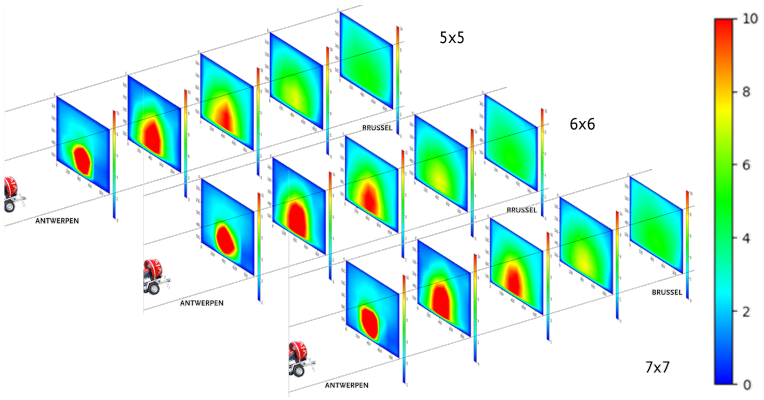

Figure 4.24: Overview of the slice files for the different grids

There are no distinct visual differences between the different grids. It can be concluded that from a visual point of view the difference between the grids is unnoticeable for the human eye, and thus this is not an efficient way of comparing the different grids. Note that these grids were measured in an empty tunnel. For a tunnel with obstacles , the chances are that one grid detects the object and the other one doesn't. Then the visual differences will be present. Although a difference is seen, this does not imply that the one grid is more accurate than the other. If an object is only detected by 1 probe, it indicates that the obstacle is too small to cause a big difference in the average velocity of the velocity profile and will be seen as an anomaly. Also for an obstacle to be seen by only one probe, it does not only have to be small but would also have to be close to the probe. In normal test set-ups, the option will always be to place the probes as far form obstacles as possible. In conclusion, it can be said that the visual comparison to determine the differences in accuracy of the different grids is not a suitable method.

4.9.6 Comparison of the average velocity between the different grids

The numerical approach to find the difference in accuracy between the different grid sizes is a more accurate approach. The average velocity of the measured cross-sections will be compared to one another. The average velocities per location are shown in Table 4.17.

The comparison was made on the basis of the difference (averaged over all the positions) between the different grids with the 7x7 grid as the reference grid because this is the finest grid. Both comparisons showed that both the average percentage and real difference for the 5x5 grid is 4 times higher than that of the 6x6 grid. The 6x6 grid has a percentage difference of 1% and a real difference of 0.04 m/s from the 7x7 grid.

The maximum real difference for the 5x5 grid is 0.26 m/s (at position 27m) and the minimum is 0.07 m/s (at position 61.4m). The maximum real difference for the 6x6 grid is -0.06 m/s (at position 27m) and the minimum is 0.02 m/s (at position 15.4m), the real difference at 61.4m equals 0.04 m/s.

Considering the results from the comparison, three conclusions can be drawn when using a measuring grid in a cross-section similar to that of the Jan De Vostunnel[3]:

- A 6x6 grid is acceptable if a 7x7 grid is not possible due to economical reasons.
- A larger grid than a 7x7 grid is for most situations not necessary hence the percentage difference between the 6x6 and the 7x7 grid is only 1%.
- In situations where the frame is placed more than 12 hydraulic tunnel diameters from the fan, a 5x5 grid might suffice.

Table 4.17: Average velocity for the different grids

	25 points	36 points	49 points
$v_{15.4}[m/s]$	3.34	3.51	3.53
$v_{27}[m/s]$	4.04	4.36	4.30
$v_{38.4}[m/s]$	4.44	4.56	4.59
$v_{50}[m/s]$	3.69	3.75	3.82
$v_{61.4}[m/s]$	3.49	3.52	3.56

4.9.7 Uncertainties of the measurements

Considering the fact that the largest part of the measurements didn't go through, there is no use in trying to calculate the uncertainty of the 6x6 and 7x7 grid. Only the 5x5 grid, where all the data is known or deduced from simulations, will be examined.

[3]For tunnels with a larger width a square based grid will not suffice. For tunnels with a large width extra research is required.

From Chapter 2 two distinct uncertainties were identified: the uncertainty of the probes and the uncertainty of velocity profile. The different uncertainties are displayed in Tables 4.18 to 4.20. The uncertainties will be discussed per measuring location.

4.9.7.1 Standard and relative uncertainty of the probes

The uncertainty interval of the probes is known and is equal to ±(0.03 m/s ± 5% of the velocity value), with a confidence interval of 95%. To evaluate the standard uncertainty interval the uncertainty should be divided by 1.96 (factor for a 95% confidence level of a normal distribution [9]).

The interval given by the manufacturer gives an idea of the largest uncertainty possible. In evaluating the uncertainty of measurements it is not realistic to work with those outer boundaries, the outer boundaries represent the standard deviation times a factor k_p to represent a confidence level of 95%. For this thesis it is important to know the uncertainty for a realistic and more probable value. The measured data should be sampled within the provided uncertainty interval, standardised by dividing with the factor 1.96 (in the assumption that a normal distribution was used).

Every measured value per probe (181 per probe) was sampled with 100 random generated samples within the standard uncertainty interval. For every measured value, the standard deviation and the relative uncertainty were calculated. The standard deviation of the samples is equal to the uncertainty of that specific measured value. The relative uncertainty is the uncertainty divided by the measured value. For every probe a sample group of 181 standard deviations and 181 relative uncertainties was created. For every probe the mean velocity, the mean of the standard deviations (unc_{pr}) and the mean of the relative uncertainties (τ_{pr}) were calculated, and this for every position. Table 4.18 shows only the uncertainty of one probe, probe 3.3. The other probes (probes 1.1-3.5) are discussed in Annex H.

Table 4.18: Uncertainties for probe 3.3 of the 5x5 grid

	$\bar{v}[m/s]$	$unc_{pr}[m/s]$	$\tau_{pr}[\%]$
$15.4m$	4.76	0.078	1.7
$27m$	4.63	0.077	1.7
$38.4m$	4.20	0.070	1.7
$50m$	3.54	0.061	1.7
$61.4m$	3.27	0.057	1.7

The uncertainty of the velocity profile is location bound since the minimum, maximum and average velocity are different for every measuring location. As described in chapter 2.3, the relative uncertainty of the velocity profile can be calculated. In the Table below a summary can be found for the different measuring locations. Note that the further the location and thus smaller fluctuations, the lower the relative uncertainty of the velocity profile.

Table 4.19: Uncertainties of the velocity profile for the 5x5 grid

	$v_{max,average}[m/s]$	$v_{min,average}[m/s]$	$\bar{v}[m/s]$	$U_{average}[-]$	$\tau_{u,average}[\%]$
$15.4m$	12.57	0.59	3.00	2.00	1.72
$27m$	9.96	1.25	3.85	1.13	1.46
$38.4m$	6.73	0.61	2.92	1.05	1.43
$50m$	4.95	1.17	2.90	0.66	1.32
$61.4m$	4.05	1.46	2.69	0.49	1.27

To have the most conservative results for the entire grid, the average relative probe(out of all the 18 probes,see Annex H) uncertainty is taken for each position. With this value and Table 4.19 the total relative uncertainty could be determined. The highest uncertainty is at position 15.4m, this is acceptable because of the turbulent zone close to the fan. The technical papers say that the measuring range from the probes is [0m/s,10m/s], because of this the higher uncertainty at the first location is explainable. At position 15.4m velocities far above the interval were measured.

Table 4.20: Total relative uncertainties for the 5x5 grid

	$\tau_{probes,mean}[\%]$	$\tau_u[\%]$	total relative uncertainty [%]
$15.4m$	2.0	1.72	2.64
$27m$	1.8	1.46	2.32
$38.4m$	1.9	1.43	2.38
$50m$	1.8	1.32	2.23
$61.4m$	1.8	1.27	2.19

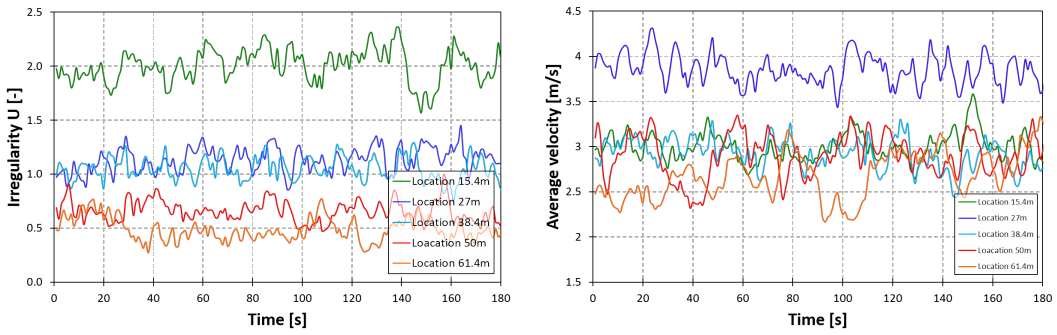

Figure 4.25: Left: Irregularity of the velocity profiles in time; Right: Average velocity in time

4.10 Comparison with the CFD simulation + Proposal for adaptation of the boundary conditions for the CFD model

The CFD simulation was set up with FDS 6.5.3[12][13]. To be able to compute the model in an accurate manner, open spaces were set up at the portals of the tunnel as cubes of

20mx24mx14m and have a cell size of 0.4mx0.4mx0.4m, all the mesh boundaries were set to be open except for the [ZMIN] boundary mesh to simulate the ground. The first 112 meters of the tunnels were modelled with a cell size of 0.2mx0.2mx0.2m and the other 628 meters were modelled with a cell size of 0.4mx0.4mx0.4m. The fan was set at a distance of 30m from the start of the tunnel and thus modelled with the same cell size as the fist 112 meters of the tunnel. A detailed description was given in chapter 4.8. The walls are 'INERT', no wind was added and no slope was modelled. The .fds-code can be found in Annex E.

4.10.1 Comparison

The measured data and the results from the simulations were compared in an attempt to improve the simulations. This was done with a visual comparison, made possible by the program FFMVisualizer, between the slice files and a numerical comparison of the average velocities per probe.

4.10.1.1 Visual comparison

In the previous chapter 4.9.5 the conclusion was drawn that a visual inspection by the human eye is not possible to determine the difference between the different grid sizes. However, for the first comparison between the measurements and the FDS simulation, the use of a visual comparison can already be very useful.

To compare the data visually, the measured data were completed using the proportions from the simulated results. Both the .csv-files for the 5x5 grid from the measurements and the FDS simulations were loaded in FFMVisualizer and afterwards the slice files were put next to each other for the comparison. Figure 4.26 shows the prepared slice files for visual comparison.

- The visual comparison highlights very clearly the difference in the jet and how fast the jet is dissipated in space. The FDS simulation shows almost no dissipation for the first 27m, whilst the measured jet is almost completely dissipated at 38.4m. Dissipation here is expressed as reaching a uniform velocity profile with the same velocity in every point of that velocity profile.
- The second visual notifiable difference is the position of the fan. During the experiment the fan was placed in the middle of the road an not the middle of the tunnel. This already made that there was an eccentricity from the exact middle of the tunnel. Although this was taken into account in the simulations, there is still a difference in the horizontal position of the fan of roughly 1m. This large contrast of the horizontal position was not the case during the test, such a big difference would have been noticed. When checking the Pyrosim file, the difference in position is in the neighbourhood of 0.5m. To investigate this error, a second and perhaps a third series of test should be performed in the same set-up.
- Third is the maximum velocity per slice file. Clearly the decay of the centreline velocity is faster for the measured data than for the simulated data.

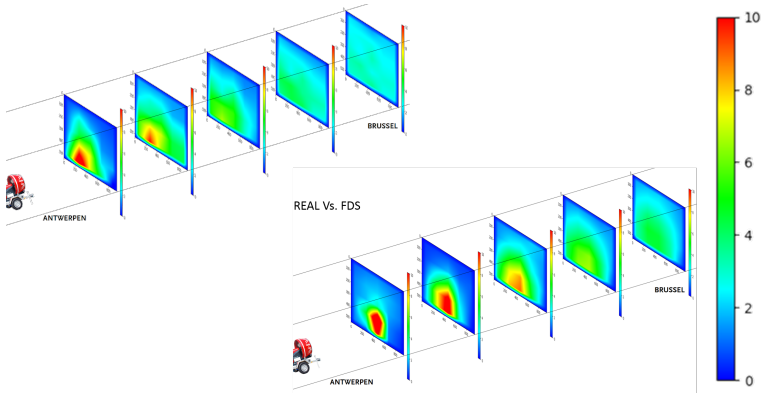

Figure 4.26: Overview of the slice files for the different grids, Left: measurements, Right: simulated results

4.10.1.2 Numerical comparison

The same method of comparing the measured data with the FDS simulations as in chapter 4.9.6 will be used in this sub chapter. The percentage differences where examined. The comparison led to a number of cases of big difference. Most of those cases are similar to those from the previous chapter (visual comparison).

Both the .csv-files for the 5x5 grid from the measurements and the FDS simulations were used for the numerical comparison.

- The average velocity for the simulation results are three of the five positions. The percentage that the average velocity of the FDS frame is higher is different for every measuring location. The list of the average percentage differences of the average probe velocities going form position 14.5m to 61.4m is as follows: [1.01, 0.6, 1.52, 1.05, 1.02]. The list of the percentage differences of the average velocities is a as follows: [0.82,0.72,1.26,1.09,1.04]. This is also illustrated in Figure 4.27.

  Notice the relatively large fluctuation of the average velocity. Normally one would expect this to be the same in the entire tunnel since no mass can go out and no mass can come in. The possible reason could be that the frame is not fine enough to measure the complete velocity profile so close to the jet. To compare average velocities in a tunnel with the simulations, the measuring frames should be placed further from the fan. This thus contradicts that to have an accurate result of the average velocity, the 5x5 grid should be placed at at least three hydraulic diameters from the disturbance as described in EN 12599. The assumption made in chapter 4.7.3 to use at least six hydraulic diameters for distance a seems to be the minimum distance from the fan when measuring a fan with the same outlet velocities as the fan used in the experiments. Note, the further the frame is installed in the tunnel the more accurately the average velocity can be calculated, this can be seen in Figure 4.27 where after 80m from the fan, the average velocity in the tunnel becomes constant. In reality it is expected to not reach the plateau because of the presence of leakage to the other tube through doors and leakage to the outside through emergency exits, so a small decay would not be unexpected.

It is still relevant to measure closely to the fan to estimate the top corner angle of the jet.

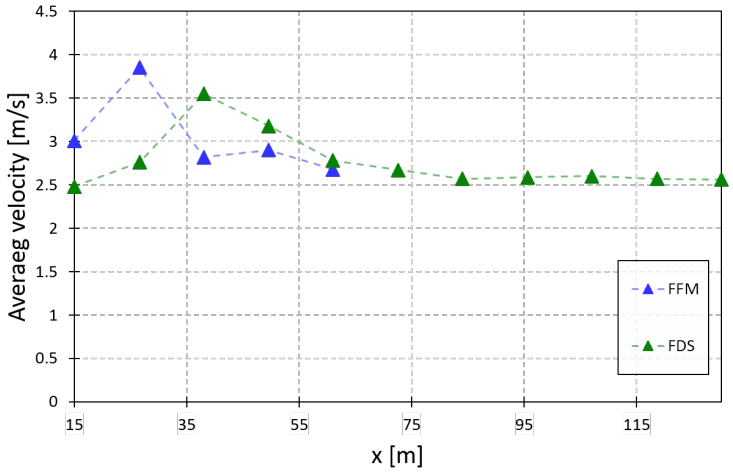

Figure 4.27: Comparison of the development of the average velocity in the tunnel between the flow field measurement (FFM) and the simulation (FDS)

- The average of percentage differences for every probe is roughly the same for the grids on positions 50m and 61.4m. This indicates that the velocity profile is becoming uniform and no large fluctuations cause big differences in velocity.
- The horizontal position of the fan in the tunnel seems to be different when looking at the probes with the highest velocities for positions 15.4m and 27m. See also the second bullet point of the previous sub chapter where this phenomenon is discussed.

The Tables in Annex I show the measured and the simulated values together with the comparison. For the real difference the data from the measurements where subtracted from the data of the FDS. The percentage difference uses the FDS data in the numerator and the measured data in the denominator .

4.10.2 Proposal for adaptation of the boundary conditions for the CFD model

Considering the visual and the numerical comparison between the measured data and the simulated data the following proposals are formulated:

- The fan was modelled as vents with no change in direction of the flow. To improve the dissipation of the jet in the simulations, the proposition is to work with louvered vents. To accomplish this the fan will have to be split up into 20 vents. The outer vents will have the largest angle, the second row of vents will have an angle between the largest angle and 0 and the middle vent will be a normal vent. The largest angle was calculated from the slice file of the measured data at position 15.4m, and is equal to 7.4°. The set-up of the louvered vents can be seen in Figure 4.28. As an indirect effect this may also result in a faster decay of the velocity in the tunnel. This adaptation was done during this thesis and the result can be seen in chapter 4.10.3.

- If after adjusting the vent, the velocity in the simulation is still to high, the use of "Synthetic Turbulence Inflow Boundary Conditions"[4] should be looked into. With adjusting the length and the number of the eddies, turbulence can be better modelled and a higher dispersion and faster decay is possible. Due to the limited time for the thesis, this could not be looked into.
- When using a multi-scale model to reduce the calculation time, the wall roughness should be adapted according to the calculated wall roughness from the Flow Field Measurements.
- In the current simulation the z-profile of the tunnel is not integrated. Since the simulation is only done in cold conditions this shouldn't have too big of an impact but to be precise it should be added as well.

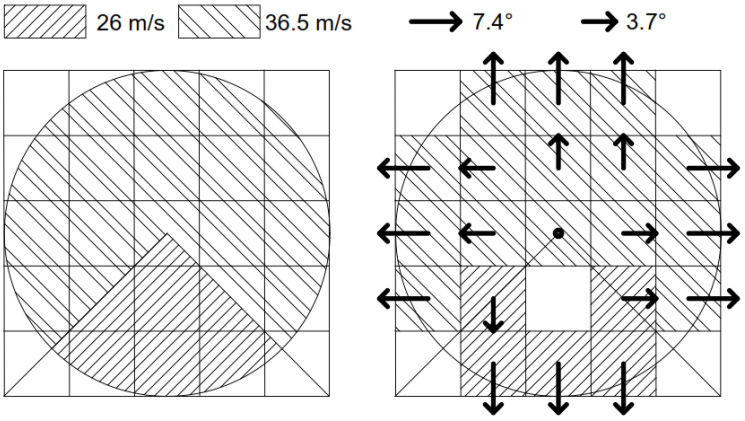

Figure 4.28: Overview of the slice files for the different grids, the direction of the arrows implies the side to where flow going out of the louvered vents are directed to with an angle of 7.4° or 3.7°, dependent on the arrow size.

4.10.3 Adapted boundary conditions of the CFD model

Adapting the boundary conditions of the CFD model by changing the fan as illustrated in Figure 4.28 showed to have a big impact on the velocity in the tunnel. In this case the velocity is being underestimated by the simulation. From this it is possible to conclude that changing the angle of the vent outlet is of big importance to correctly model the fan. When remodelling the fan, the shroud that had a length of 40cm was deleted, in this manner the angled flow could develop properly.

The design of the fan can be seen in Figure 4.29 and Figure 4.30

[4]This is described in detail in Chapter 9.1.8 of the FDS USer Guide [13]

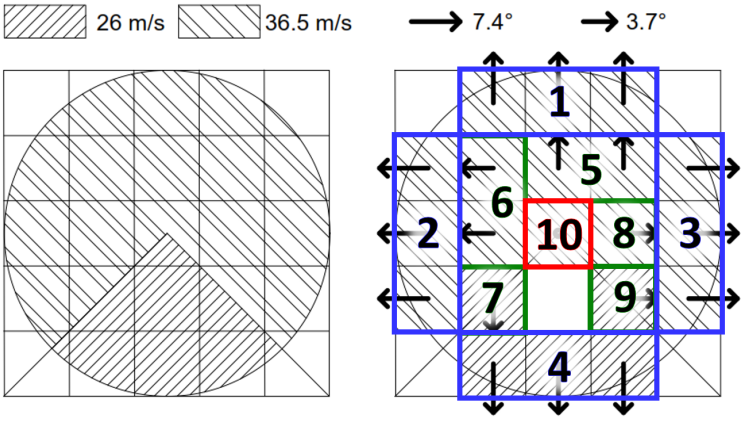

Figure 4.29: Subdivision of the fan

```
&SURF ID='LOUVER_1', VEL=-36.195,VEL_T=0.0,4.7, TAU_V=5.0,COLOR='GREEN' /
&SURF ID='LOUVER_2', VEL=-36.195,VEL_T=4.7,0.0, TAU_V=5.0,COLOR='GREEN' /
&SURF ID='LOUVER_3', VEL=-36.195,VEL_T=-4.7,0.0, TAU_V=5.0,COLOR='GREEN' /
&SURF ID='LOUVER_4', VEL=-36.195,VEL_T=0.0,-4.7, TAU_V=5.0,COLOR='GREEN' /
&SURF ID='LOUVER_5', VEL=-36.319,VEL_T=0.0,3.625, TAU_V=5.0,COLOR='GREEN' /
&SURF ID='LOUVER_6', VEL=-36.319,VEL_T=3.625,0.0, TAU_V=5.0,COLOR='GREEN' /
&SURF ID='LOUVER_7', VEL=-25.871,VEL_T=2.58,0.0, TAU_V=5.0,COLOR='GREEN' /
&SURF ID='LOUVER_8', VEL=-36.319,VEL_T=-3.625,0.0, TAU_V=5.0,COLOR='GREEN' /
&SURF ID='LOUVER_9', VEL=-25.871,VEL_T=-2.58,0.0, TAU_V=5.0,COLOR='GREEN' /

&VENT ID='VENT_OUT_1', SURF_ID='LOUVER_1', XB=30.4,30.40,-0.6,0.0,1.8,2.0, COLOR='BLUE'/
&VENT ID='VENT_OUT_2', SURF_ID='LOUVER_2', XB=30.4,30.40,0,0.2,1.2,1.8, COLOR='BLUE'/
&VENT ID='VENT_OUT_3', SURF_ID='LOUVER_3', XB=30.4,30.40,-0.8,-0.6,1.2,1.8, COLOR='BLUE'/
&VENT ID='VENT_OUT_4', SURF_ID='LOUVER_4', XB=30.4,30.40,-0.6,0.0,1.0,1.2, COLOR='BLUE'/
&VENT ID='VENT_OUT_5', SURF_ID='LOUVER_5', XB=30.4,30.40,-0.6,-0.2,1.6,1.8, COLOR='BLUE'/
&VENT ID='VENT_OUT_6', SURF_ID='LOUVER_6', XB=30.4,30.40,-0.2,0.0,1.4,1.8, COLOR='BLUE'/
&VENT ID='VENT_OUT_7', SURF_ID='LOUVER_7', XB=30.4,30.40,-0.2,0.0,1.2,1.4, COLOR='BLUE'/
&VENT ID='VENT_OUT_8', SURF_ID='LOUVER_8', XB=30.4,30.40,-0.6,-0.4,1.2,1.4, COLOR='BLUE'/
&VENT ID='VENT_OUT_9', SURF_ID='LOUVER_9', XB=30.4,30.40,-0.6,-0.4,1.4,1.6, COLOR='BLUE'/
&VENT ID='VENT_OUT_10', SURF_ID='HVAC', XB=30.4,30.40,-0.4,-0.2,1.4,1.6, COLOR='BLUE'/

&HVAC ID='Node_10_01', TYPE_ID='NODE', DUCT_ID='Duct_10', VENT_ID='VENT_IN_10'/
&HVAC ID='Node_10_02', TYPE_ID='NODE', DUCT_ID='Duct_10', VENT_ID='VENT_OUT_10'/
&HVAC ID='Duct_10', TYPE_ID='DUCT', DIAMETER=0.451352, FAN_ID='FAN_10', NODE_ID='Node_10_01','Node_10_02', ROUGHNESS=1.0E-3/

&HVAC ID='FAN_10', TYPE_ID='FAN', VOLUME_FLOW=1.44/
```

Figure 4.30: CFD code of the fan, the numbers refer to those from Figure 4.29

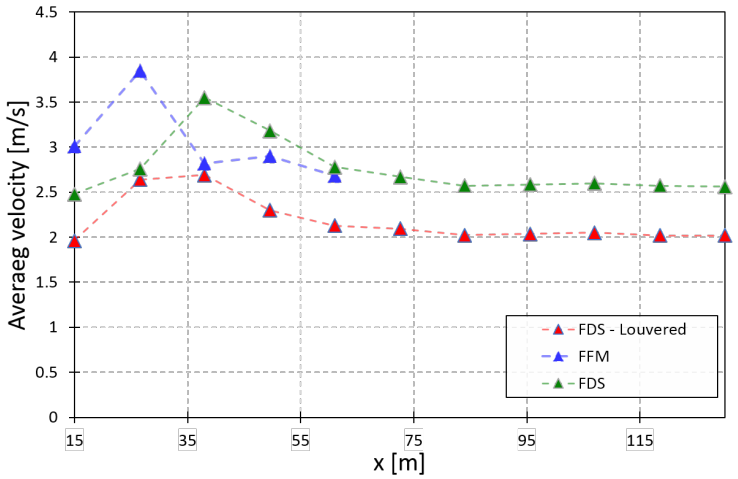

Figure 4.31: Comparison of the development of the average velocity in the tunnel between the flow field measurement (FFM),the original simulation (FDS) and the adapted simulation (FDS-Louvered)

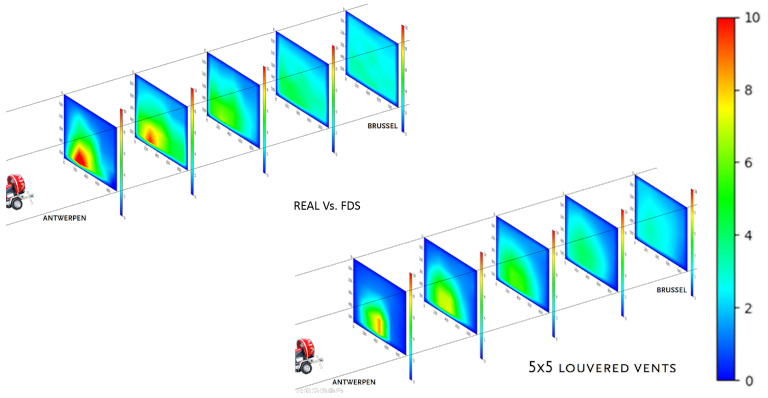

Figure 4.32: Overview of the slice files for the different grids, Left: measurements, Right: simulated results

4.11 Cost-Benefit analysis

To complete the research a cost-benefit analysis was performed to determine the most beneficial measuring method from an economical and engineering point of view. Figure 4.33 shows a comparison between four different measuring methods. The considered measuring methods are the EN 12599, EN ISO 5802 - S (separate measurements to map the entire velocity profile by moving the frame horizontal, as is done in this thesis), EN ISO 5802 and S21-208-2. The analysis is based on five criteria:

- Material cost
- Set-up time
- Measuring time

- Repeatability
- Accuracy

The scale used to determine the weight of the criteria goes from 1 to 5, with 5 being "High" and 1 being "Low". Analysing the different methods highlighted the poor quality of the "loop method" used in S21-205-2, performing the lowest of all four. The method used in EN ISO 5802 with a complete frame has the highest level of accuracy but also the biggest cost. With an equal cost but a lower level of accuracy, EN 12599 is placed as third best. The second best method for accuracy is the one being used in this thesis, but with a significant lower cost than the method with a full frame (EN ISO 5802).

It can thus be concluded that the method used in the thesis (EN ISO 5802 with moving a smaller frame horizontally) comes out as best in the cost-benefit analysis.

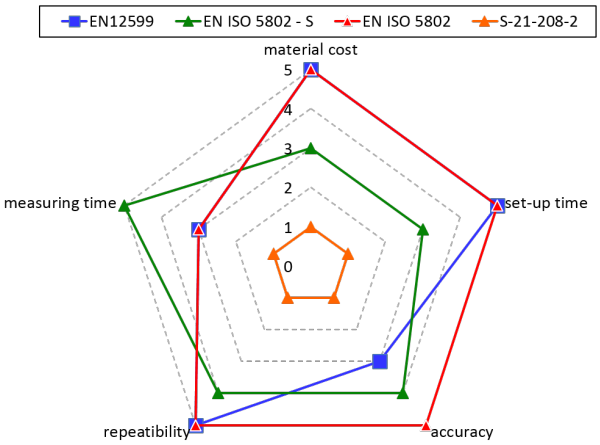

Figure 4.33: Comparison of the different measuring methods, based on five criteria

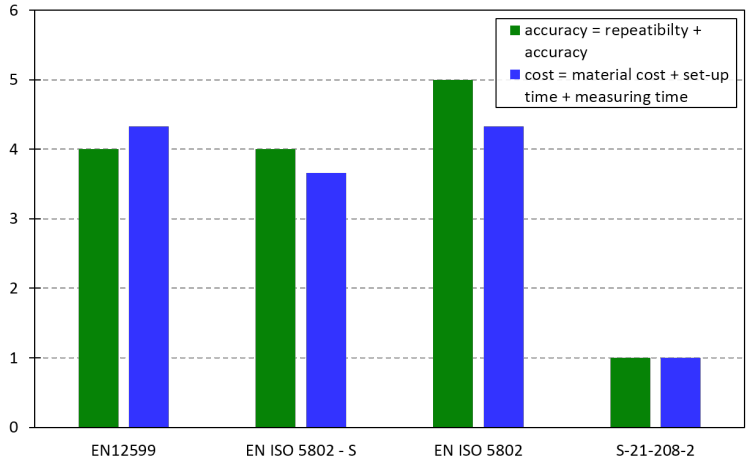

Figure 4.34: Comparison of the different measuring methods, based on two criteria

Chapter 5

Conclusion

After investigation of the different codes describing how to measure the velocity profile in a duct induced by a fan, the Log-Tchebycheff method described in ISO 5802 is the most realistic. This method takes into account the steep raise in velocity from the boundaries (where the velocity is equal to 0 $[m/s]$) to a zone close to the boundaries, and is recommended to use for both tunnels and car parks. For this method to be valid, the grid should be measured in a cross-section where 4 boundaries (2 walls, a floor and a ceiling) are present. To determine the uncertainties of the measured velocity profiles, code EN 12599 was considered. The code proposed a table for a predetermined level of uncertainty of the irregularity of the velocity profile and a formula to calculate that uncertainty precisely. Both codes are complementary to each other and should both be used when performing flow field measurements.

With an average relative difference between the 6x6 grid and the 7x7 grid of 1%, the conclusion can be made that for a tunnel or a portal in a car park with similar or smaller measurements a 6x6 grid will suffice to have accurate results to compare with the simulations. For larger cross-sections further research is necessary. For the determination of the average velocity the measuring frame should be placed far enough from the fan to decrease the uncertainty of the average velocity. To investigate the angle of top corner angle of the jet, its is relevant to measure closer to the fan.

The deployment of mobile fans in an incident tunnel was proven to be effective. Dependent on the tunnel geometry, the wind influence, obstacles in the tunnel and the slope of the tunnel, one or more fans are needed to succeed in generating a smoke free passage way for the fire fighters to reach the fire. For small tunnels it is advised to deploy the fans in parallel, note that fire fighters would still have to be able to pass without being hindered too much by the jet of the fans. For long tunnels, the linear pressure losses will be larger and the fans will be placed in series to increase the pressure rise. For the specific fans used in the experiments the minimal distance in between two fans was 10 times the hydraulic diameter of the tunnel. The use of mobile fans during an intervention is not only applicable for tunnels where a ventilation system is absent, but can also improve the tenability conditions in tunnels with a working ventilation system. The deployment of mobile fans for large fires with a high HRR should always be pursued, but with taking into account that a substantial back-layering could exist and the large heat fluxes that come with it.

The wall roughness calculation highlighted the significant importance of performing wall roughness calculations in advance of designing the ventilation system in a tunnel with a 1D model. Thus, it is important to stress that before a ventilation study is performed for a tunnel with a non-regular cross-section and/or with repeated large obstructions on the ceiling/walls, the wall roughness could accurately be determined using a mobile fan together with the necessary pressure measurements. In this manner the uncertainty of the wall roughness can be reduced and a more accurate design can be accomplished. This is not only relevant for a 1D model but will also be a large added value when working with a multi-scale model. If possible, it deems best to also do preliminary tests of the fan(s) in situ to determine the actual velocity before modelling the complete tunnel or car park.

The visual comparison between the flow field measurements and the simulated data is useful for a first check to highlight distinct differences, it helps narrowing down the field where the focus should be put on during the numerical comparison. The numerical comparison is necessary to detect discrepancies in the simulated data.

Using louvered vents to model the jet fan is necessary to create a more accurate simulation. The use of "Synthetic Turbulence Inflow Boundary Conditions" should be looked into. With adjusting the length and the number of the eddies, turbulence can be better modelled and a higher dispersion and faster decay is possible. Due to the limited time for the thesis, this could not be looked into.

Further research would make it possible to create a rule of thumb that would allow the user for a faster determination of the grid size for the flow field measurements. One would then have to do a sensitivity analysis for the modelling of a fan(s) in a tunnel or car park to find the minimum required cell size, and with the rule of thumb the required grid size could be determined.

Bibliography

[1] CEN, *NBN EN 12599: Ventilation for buildings - Test procedures and measurement methods to hand over air conditioning and ventilaiton systems.* CEN, Avenue Marnix 17, B-1000 Brussels, second ed., December 2012.

[2] CEN, *NBN EN ISO 5802: Industrial fans - Performance testing in situ (ISO 5802:2001).* CEN, Rue de Stassart 36, B-1050 Brussels, first ed., March 2009.

[3] B. voor Normalisatie, *NBN S 21-208-2: brandbeveiliging in gebouwen - Ontwerp van rook - en warmteafvoersystemeen (RWA) van gesloten parkeergebouwen.* Bureau voor Normalisatie, Jozef II-straat 40, 1000 Brussels, third ed., July 2014.

[4] H. I. Ying Zhen Li, Bo Lei, "Study of critical velocity and backlayering length in longitudinally venitlated tunnel fires," *Fire Safety Journal 45*, pp. 361–370, 2010.

[5] S. Tunnelveiligheid, *Aanbevelingen Ventilatie Van Verkeerstunnels.* Thieme GrafiMedia Groep, Deventer, December 2005. p110-p111.

[6] J. L. Julien Veyet, "Development of an original measurement method for the toulouse metro (france)," *8th International Conference 'Tunnel Safety and Ventilation' Graz*, pp. 173–180, 2016.

[7] J. S. K. C. Witt, ""bend it like a banana"," *12th symposium on Aerodynamics, Ventilation Fire in Tunnels*, vol. 2, pp. 683–693, 2006.

[8] D. B. M. B. G. Clark, D. Suansbury, "Performance evaluation of jet fan deflectors for road tunnel longitudinal ventilation," *15th symposium on Aerodynamics, Ventilation Fire in Tunnels*, pp. 9–26, 2013.

[9] JCGM, *Evaluation of measurement data - Guide to the expression of uncertainty in measurement.* JCGM, first ed., September 2008.

[10] B. Daly, *Woods Pracitcal Guide to Fan Engineering.* Woods of Colchester Limited, sixth ed., 1992.

[11] S. K. Wang, *Handbook of Air Conditioning and Refrigeration.* McGraw-Hill, first ed., 2001.

[12] R. M. Kevin McGrattan, Simo Hostikka, *Fire Dynamics Simulator Technical Reference Guide Volume 1: Mathematical Model.* NIST SPecial Publication 1018, 2017.

[13] R. M. Kevin McGrattan, Simo Hostikka, *Fire Dynamics Simulator Users Guide.* NIST SPecial Publication 1019, 2017.

[14] M. B. Y. Wu, "Control of smoke flow in tunnel fires using longitudinal ventilation systems - a study of critical velocity," *Fire Safety Journal 35*, no. 363-390, 2000.

[15] Y. W. G.T. Atkinson, "Smoke control in sloping tunnels," *Fire Safety Journal 27*, no. 335-341, 1996.

[16] X. D. Matteo Pachera, Bart Van Weyenberge, *DEVELOPMENT OF A FULL PROBABILISTIC RISK MODEL TO ASSESS THE PERFORMANCE OF LONGITUDINAL VENTILATION SYSTEM FOR FIRES IN TUNNEL*, April 2018.

[17] B. Merci, "One-dimensional analysis of the global chimney effect in case of fire in an inclined tunnel," *Fire Safety Journal 43*, pp. 376–389, 2008.

[18] R. B. F.Tarada *Proceedings of 13th symposium on Aerodynamics and Ventilation of Vehicle Tunnels. BHRG. New brunswick, New Jersey, USA*, pp. 95–107, 2009.

[19] A. B. Richard Carvel, *Handbook of Tunnel Fire Safety.* ICE Publishing, second ed., 2005.

[20] "https://www.pipeflowcalculations.com/pipe-valve-fitting-flow/flow-in-pipes.php."

[21] K. K. Y. Guan Heng Yeah, *Computional Fluid Dynamics in Fire Engineering.* Butterworth-Heinemann, first ed., 2009.